Chinese Journal of Aeronautics, (2024), xxx(xx): xxx–xxx

Chinese Society of Aeronautics and Astronautics
& Beihang University

Chinese Journal of Aeronautics

cja@buaa.edu.cn
www.sciencedirect.com

FULL LENGTH ARTICLE

An efficient uncertainty propagation method for nonlinear dynamics with distribution-free P-box processes

Licong ZHANG[a], **Chunna LI**[a], **Hua SU**[a], **Yuannan XU**[b], **Andrea Da RONCH**[c], **Chunlin GONG**[a,*]

[a] *Flight Vehicle Design Key Laboratory, School of Astronautics, Northwestern Polytechnical University, Xi'an 710072, China*
[b] *Research and Development Department, China Academy of Launch Vehicle Technology, Beijing 100076, China*
[c] *Faculty of Engineering and Physical Sciences, University of Southampton, Southampton, England SO171BJ, UK*

Received 9 October 2023; revised 15 November 2023; accepted 6 February 2024

KEYWORDS

Nonlinear dynamics;
Uncertainty propagation;
Imprecise probability;
Distribution-free P-box processes;
Chebyshev method

Abstract The distribution-free P-box process serves as an effective quantification model for time-varying uncertainties in dynamical systems when only imprecise probabilistic information is available. However, its application to nonlinear systems remains limited due to excessive computation. This work develops an efficient method for propagating distribution-free P-box processes in nonlinear dynamics. First, using the Covariance Analysis Describing Equation Technique (CADET), the dynamic problems with P-box processes are transformed into interval Ordinary Differential Equations (ODEs). These equations provide the Mean-and-Covariance (MAC) bounds of the system responses in relation to the MAC bounds of P-box-process excitations. They also separate the previously coupled P-box analysis and nonlinear-dynamic simulations into two sequential steps, including the MAC bound analysis of excitations and the MAC bounds calculation of responses by solving the interval ODEs. Afterward, a Gaussian assumption of the CADET is extended to the P-box form, i.e., the responses are approximate parametric Gaussian P-box processes. As a result, the probability bounds of the responses are approximated by using the solutions of the interval ODEs. Moreover, the Chebyshev method is introduced and modified to efficiently solve the interval ODEs. The proposed method is validated based on test cases, including a duffing oscillator, a vehicle ride, and an engineering black-box problem of launch vehicle trajectory. Compared to the reference solutions based on the Monte Carlo method, with relative errors of less than 3%, the pro-

* Corresponding author.
E-mail address: leonwood@nwpu.edu.cn (C. GONG).
Peer review under responsibility of Editorial Committee of CJA.

ELSEVIER Production and hosting by Elsevier

https://doi.org/10.1016/j.cja.2024.05.028
1000-9361

Please cite this article in press as: ZHANG L et al. An efficient uncertainty propagation method for nonlinear dynamics with distribution-free P-box processes, *Chin J Aeronaut* (2024), https://doi.org/10.1016/j.cja.2024.05.028

posed method requires less than 0.2% calculation time. The proposed method also possesses the ability to handle complex black-box problems.

1. Introduction

The dynamic response evaluation of nonlinear systems is critical in most engineering problems. Due to the unavoidable uncertainty in practical applications, evaluating the response solely under deterministic and precise conditions is inadequate. Therefore, the Uncertainty Propagation (UP) in nonlinear dynamics has become a research focus in recent years.[1,2] The task of the UP analysis is to calculate the uncertainty characteristics of system responses based on the quantification models of input uncertainties. Different sources of uncertainties are generally represented by different models. Aleatory uncertainties, arising from the inherent physical randomness of systems and excitations, can be represented by the probabilistic model, when sufficient and precise data are available. However, the uncertainties resulting from limited or poor-quality data, termed imprecision (a form of epistemic uncertainties), have to be represented by non-probabilistic models.[3] When aleatory uncertainties and imprecision appear together and result in imprecise probabilistic information, both probabilistic and non-probabilistic models are inapplicable. In such instances, imprecise probabilities[4] serve as suitable models for representation. Under these different types of uncertainty models, the corresponding UP analyses for dynamical systems have also been investigated.

Under the probabilistic model, uncertainties are quantified using precise probability distributions, and the uncertain systems can be formulated as nonlinear stochastic dynamics. In this field, a great number of classical analysis methods have been developed, such as the Monte Carlo (MC) method,[5] local linearization method,[6] stochastic linearization method,[7] stochastic average method,[8] path-integration method,[9] Hamiltonian formulation[10] and so on. Recently, the integration methods based on probability conservation, including probability density evolution method[11] and direct probability integral method,[12,13] have become a focus. Several surrogate-model-based methods have also been investigated, including Polynomial chaos expansion,[14,15] Kriging,[16] and artificial neutral networks,[17,18] as well as dimension reduction approaches[19] for high-dimensional surrogate-modelling. Frequency-domain methods[20,21] have also been recognized as powerful tools for stochastic-dynamic analyses. Some other methods have proven effective in specific fields; for instance, the unscented transformation,[22] state transition tensors,[23] and Gaussian mixture models[24] have been widely applied in flight mechanics. Moreover, numerous novel methods[25–27] have been successively developed. Although these probabilistic methods have achieved success in solving various UP problems, they still face the challenge that collecting sufficient information for constructing precise probability distributions of uncertainties may not always be possible.

Non-probabilistic models[3,28,29] can operate effectively without relying on probabilistic information. The convex model,[28] in particular, is the most well-known and is widely applied in the study of nonlinear dynamics. Wu et al.[30,31] introduced the Chebyshev interval method for UP analysis of nonlinear dynamics. Then, Li et al.[32] proposed a sparse regression method to improve the efficiency of the Chebyshev method. Wang et al.[33,34] developed a Legendre-polynomial-based method to propagate interval uncertainties in nonlinear dynamics. These methods have been applied to a number of engineering problems.[35,36] However, they cannot handle correlated or time-varying uncertainties, which commonly exist in dynamical systems. Therefore, to quantify the correlation of intervals, several improved convex models[37–39] have been proposed. For time-varying intervals, Jiang et al.[40] proposed a novel quantification model, namely the interval process. Based on the interval process, various methods have been presented for UP analyses of linear systems.[41] Subsequently, for nonlinear systems, an MC-simulation method,[42] the Karhunen-Loève expansion method,[43] and a linearization method[44] have been gradually proposed.

Imprecise probabilistic information is also common in practice, where imprecise probabilities are considered a more appropriate quantification model. The P-box[45] may serve as a popular representative of imprecise probabilities. The P-box has been investigated in numerous static uncertainty analysis problems;[46–48] however, it has only recently gained interest for dynamical problems. The quantification models of dynamical uncertainties have been investigated by using the P-box model. Li[49] and Faes[50] et al. proposed the definitions of parametric and distribution-free (non-parametric) P-box processes, respectively, to describe time-varying uncertainties. Meanwhile, several UP methods have been proposed for dynamical problems. Faes and Moens[51] studied imprecise random fields with parametrized kernel functions in linear dynamics. The authors also developed analysis methods for estimating the imprecise first excursion probabilities in linear dynamics.[52,53] Faes et al.[54] further proposed an operator-norm-based method to calculate the imprecise probabilities. However, these methods are only valid for linear dynamics. For nonlinear dynamics, very few approaches have been developed. Enszer et al.[55] applied the Taylor expansion model to calculate the probability bounds for nonlinear dynamics. Ni et al.[56] proposed an operator norm-based statistical linearization method for bounding the first excursion probability of nonlinear structures. However, it should be noted that all of the aforementioned methods have only considered the parametric P-boxes or processes. Because it is not always possible to obtain a complete parametric description of P-boxes, distribution-free P-box problems are also considered significant. However, in this field, only Faes et al.[50] suggested a propagation method when defining the distribution-free P-box process, and this technique is only suitable for linear dynamics. There is still a lack of appropriate UP approaches for nonlinear problems with distribution-free P-box processes.

In this work, the nonlinear dynamics with distribution-free P-box processes is investigated and an efficient UP method for the nonlinear dynamics is proposed. The major contributions of this work are as follows:

(1) The UP problem of nonlinear dynamics with distribution-free P-box processes is first proposed and defined. This problem is critical, as the precise probabilistic information of excitations of nonlinear dynamics is always challenging to obtain in practical engineering.
(2) A novel UP method is developed. The P-box analyses of excitations and stochastic analyses of nonlinear systems are decoupled by using the Covariance Analysis Describing Equation Technique (CADET). This significantly improves the efficiency of the UP analysis. Based on the method, the bounds of the means and covariances of the system responses, as well as their probability bounds, can be obtained.
(3) The Chebyshev method is introduced to non-intrusively solve the interval analyses in the UP procedure and further improve the UP analysis efficiency.

The rest of this paper is organized as follows. In Section 2, several issues about nonlinear dynamics with distribution-free P-box processes are discussed. Section 3 introduces the proposed UP method in detail. The proposed method is tested by using two numerical examples and a Launch-Vehicle (LV) ascent-trajectory problem in Section 4. Finally, the conclusions are presented in Section 5.

2. Nonlinear dynamics with distribution-free P-box processes

Consider an N-degree-of-freedom nonlinear dynamic with an $M-$dimensional time-varying uncertain excitation. This can be mathematically expressed as follows:

$$\dot{\mathrm{X}}(t) = \mathrm{f}(\mathrm{X}, t) + \mathrm{B}(t)\mathrm{W}(t) \tag{1}$$

where $\mathrm{W}(t) = [W_1(t),\ W_2(t),\ \ldots,\ W_M(t)]^{\mathrm{T}}$, denotes the $M-$dimensional vector comprising the stochastic excitations; $\mathrm{X}(t) = [X_1(t),\ X_2(t),\ \ldots,\ X_N(t)]^{\mathrm{T}}$, denotes the N-dimensional vector comprising the state variables of the system; $\mathrm{f}(\cdot) = [f_1(\cdot),\ f_2(\cdot),\ \ldots,\ f_N(\cdot)]^{\mathrm{T}}$, denotes the nonlinear vector function that describes the system; and $\mathrm{B}(t)$ denotes the N by M input matrix. Under the probabilistic model, the time-varying uncertain excitations, i.e., $W_m(t)$ ($m = 1, 2, \ldots, M$), can be described as stochastic processes. However, in practical engineering cases, it may not always be possible to obtain precise probabilistic information about these excitations. To address this issue, the P-box process was proposed to quantify the time-varying excitations with imprecise probabilistic information. The detailed concept of the P-box process will be introduced in the following subsection.

2.1. Definition of distribution-free P-box processes

Before introducing the P-box process, the basic definition of static P-box is given first. The P-box variable $W^{\mathrm{P.B.}}$, with the superscript P.B. denoting the P-box, is described by the two Cumulative-Distribution-Function (CDF) bounds, i.e., a lower CDF $F_W^{\mathrm{L}}(\cdot)$ and an upper CDF $F_W^{\mathrm{U}}(\cdot)$, as follows:

$$F_W^{\mathrm{L}}(\omega) \leqslant F_W(\omega) \leqslant F_W^{\mathrm{U}}(\omega) \tag{2}$$

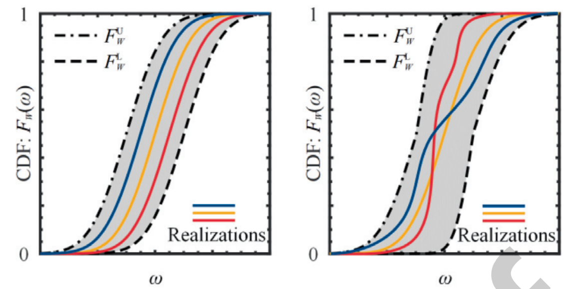

(a) Parametric P-box (b) Distribution-free P-box

Fig. 1 Visual depiction of the P-box.

where $F_W(\cdot)$ denotes a possible CDF realization of the imprecise CDF bounded by $F_W^{\mathrm{L}}(\cdot)$ and $F_W^{\mathrm{U}}(\cdot)$. Therefore, the P-box variable $W^{\mathrm{P.B.}}$ could be denoted by its CDF bounds as $[F_W^{\mathrm{L}},\ F_W^{\mathrm{U}}]$, with all P-boxes that appear later in the text denoted in a similar fashion.

P-box variables are typically categorized as parametric P-box and distribution-free (non-parameterized) P-box, as shown in Fig. 1(a) and (b), respectively. The distribution type of a parametric P-box is known; however, the distribution parameters are imprecise. The distribution-free P-box lacks precise information in terms of both the distribution type and parameters. This work focuses on the distribution-free type of P-box variables, as it is common, in practical engineering, that a complete parametric description of the distributions of probability bounds cannot be obtained.

When a distribution-free P-box is time-varying, it will become a distribution-free P-box process whose CDFs are distribution-free P-boxes at all times, as shown in Fig. 2. A study[50] recently proposed a mathematical definition based on translation theory:

$$W^{\mathrm{P.B.}}(t) = \left[\left(F_W^{\mathrm{L}}\right)^{-1}, \left(F_W^{\mathrm{U}}\right)^{-1}\right]^{\circ}\Phi(N(t)) \tag{3}$$

where $\circ$ denotes the operator of composite mapping, $[F_W^{\mathrm{L}},\ F_W^{\mathrm{U}}]$ denotes a distribution-free P-box, $N(t)$ denotes a Gaussian stochastic process with zero mean and unit variance, and $\Phi(\cdot)$ denotes the standard normal CDF. The expression presented in Eq. (3) defines the CDF bounds of the imprecise stochastic process at any time by $[F_W^{\mathrm{L}},\ F_W^{\mathrm{U}}]$ and the time-correlation structure by $N(t)$.

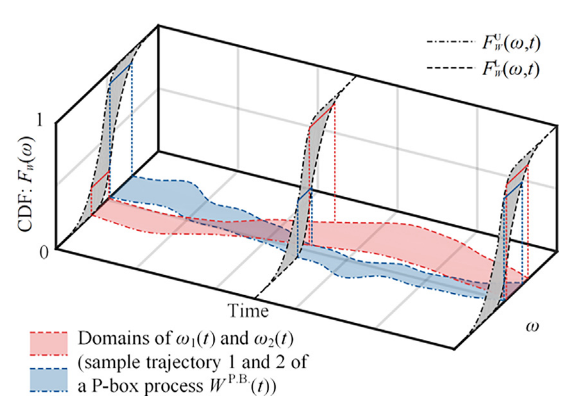

Fig. 2 Visual depiction of the P-box process.

Please cite this article in press as: ZHANG L et al. An efficient uncertainty propagation method for nonlinear dynamics with distribution-free P-box processes, *Chin J Aeronaut* (2024), https://doi.org/10.1016/j.cja.2024.05.028

As shown in Fig. 2, the sample trajectories of a distribution-free P-box process $W^{\mathrm{P.B.}}(t)$ are no longer precise functions over time, but interval-valued functions. Accordingly, the mean and variance of $W^{\mathrm{P.B.}}(t)$, denoted by $\mu_W^{\mathrm{I}}(t)$ and $(\sigma_W^2)^{\mathrm{I}}(t)$, respectively, are both interval-valued functions over time, with the superscript I denoting the interval. If $N(t)$ in Eq. (3) is a stationary Gaussian process, $\mu_W^{\mathrm{I}}(t)$ and $(\sigma_W^2)^{\mathrm{I}}(t)$ will become constant intervals as denoted by μ_W^{I} and $(\sigma_W^2)^{\mathrm{I}}$, respectively. This can be mathematically expressed as follows:

$$\begin{cases} \mu_W^{\mathrm{I}} = \left[\min\limits_{F_W \in \left[F_W^{\mathrm{L}}, F_W^{\mathrm{U}}\right]} \mathrm{mean}(F_W), \max\limits_{F_W \in \left[F_W^{\mathrm{L}}, F_W^{\mathrm{U}}\right]} \mathrm{mean}(F_W)\right] \\ (\sigma_W^2)^{\mathrm{I}} = \left[\min\limits_{F_W \in \left[F_W^{\mathrm{L}}, F_W^{\mathrm{U}}\right]} var(F_W), \max\limits_{F_W \in \left[F_W^{\mathrm{L}}, F_W^{\mathrm{U}}\right]} var(F_W)\right] \end{cases} \tag{4}$$

where $\mathrm{mean}(\cdot)$ and $var(\cdot)$ denote the operators for calculating the mean and variance of the given CDF realization F_W, respectively, which can be expressed as follows:

$$\begin{cases} \mathrm{mean}(F_W) = \int_{-\infty}^{\infty} (F_W)^{-1} \circ \Phi(\eta) d(\Phi(\eta)) \\ var(F_W) = \int_{-\infty}^{\infty} \left((F_W)^{-1} \circ \Phi(\eta) - \mathrm{mean}(F_W)\right)^2 d(\Phi(\eta)) \end{cases} \tag{5}$$

where η denotes the integration variable.

2.2. Uncertainty propagation problems under P-box processes

If only the CDF-bound information of the excitations for the nonlinear system presented in Eq. (1) are available, they can be described as distribution-free P-box processes, as follows:

$$\mathrm{W}^{\mathrm{P.B.}}(t) = \left[W_1^{\mathrm{P.B.}}(t), W_2^{\mathrm{P.B.}}(t), \dots, W_M^{\mathrm{P.B.}}(t)\right]^{\mathrm{T}} \tag{6}$$

To define $W_m^{\mathrm{P.B.}}(t)$ ($m = 1, 2, \dots, M$) based on Eq. (3), M static P-boxes are given as $[F_{W_m}^{\mathrm{L}}, F_{W_m}^{\mathrm{U}}]$ ($m = 1, 2, \dots, M$). For simplicity, the M P-boxes are represented in vector form $[\mathrm{F}_{\mathrm{W}}^{\mathrm{L}}, \mathrm{F}_{\mathrm{W}}^{\mathrm{U}}]$, where $\mathrm{F}_{\mathrm{W}}^{\mathrm{L}} = \left[\mathrm{F}_{W_1}^{\mathrm{L}}, \mathrm{F}_{W_2}^{\mathrm{L}}, \dots, \mathrm{F}_{W_M}^{\mathrm{L}}\right]^{\mathrm{T}}$ and $\mathrm{F}_{\mathrm{W}}^{\mathrm{U}} = \left[\mathrm{F}_{W_1}^{\mathrm{U}}, \mathrm{F}_{W_2}^{\mathrm{U}}, \dots, \mathrm{F}_{W_M}^{\mathrm{U}}\right]^{\mathrm{T}}$.

Under $\mathrm{W}^{\mathrm{P.B.}}(t)$, the nonlinear dynamical system can be expressed as follows:

$$\dot{\mathrm{X}}^{\mathrm{P.B.}}(t) = \mathrm{f}(\mathrm{X}^{\mathrm{P.B.}}(t), t) + \mathrm{B}(t)\mathrm{W}^{\mathrm{P.B.}}(t) \tag{7}$$

The responses of the nonlinear system $\mathrm{X}^{\mathrm{P.B.}}(t)$ also become P-box processes. Therefore, the main objective of the UP analysis is to obtain the CDF bounds of the responses, denoted by $[\mathrm{F}_{\mathrm{X}}^{\mathrm{L}}, \mathrm{F}_{\mathrm{X}}^{\mathrm{U}}]$, at any time instant t. This can be mathematically expressed as follows:

$$\begin{cases} \mathrm{F}_{\mathrm{X}}^{\mathrm{L}}(\mathrm{x}|t) = \min\limits_{\mathrm{F}_{\mathrm{W}} \in \left[\mathrm{F}_{\mathrm{W}}^{\mathrm{L}}, \mathrm{F}_{\mathrm{W}}^{\mathrm{U}}\right]} \mathrm{F}_{\mathrm{X}}(\mathrm{x}|\mathrm{F}_{\mathrm{W}}, t) \\ \mathrm{F}_{\mathrm{X}}^{\mathrm{U}}(\mathrm{x}|t) = \max\limits_{\mathrm{F}_{\mathrm{W}} \in \left[\mathrm{F}_{\mathrm{W}}^{\mathrm{L}}, \mathrm{F}_{\mathrm{W}}^{\mathrm{U}}\right]} \mathrm{F}_{\mathrm{X}}(\mathrm{x}|\mathrm{F}_{\mathrm{W}}, t) \end{cases} \tag{8}$$

where F_{W} represents the realizations of the P-boxes $[\mathrm{F}_{\mathrm{W}}^{\mathrm{L}}, \mathrm{F}_{\mathrm{W}}^{\mathrm{U}}]$ that define the P-box processes $\mathrm{W}^{\mathrm{P.B.}}(t)$. Meanwhile, the evaluation of failure probability bounds is considered an important task. When the first-passage problem[25] is considered, this can be mathematically expressed as follows:

$$\begin{cases} P^{\mathrm{L}} = \min\limits_{\mathrm{F}_{\mathrm{W}} \in \left[\mathrm{F}_{\mathrm{W}}^{\mathrm{L}}, \mathrm{F}_{\mathrm{W}}^{\mathrm{U}}\right]} \Pr\left\{\max\limits_{t \in [0,T]} (|X(t|\mathrm{F}_{\mathrm{W}})|) > \delta\right\} \\ P^{\mathrm{U}} = \max\limits_{\mathrm{F}_{\mathrm{W}} \in \left[\mathrm{F}_{\mathrm{W}}^{\mathrm{L}}, \mathrm{F}_{\mathrm{W}}^{\mathrm{U}}\right]} \Pr\left\{\max\limits_{t \in [0,T]} (|X(t|\mathrm{F}_{\mathrm{W}})|) > \delta\right\} \end{cases} \tag{9}$$

where P^{L} and P^{U} denote the lower and upper bounds of the first-passage probability, respectively; $\Pr\{\cdot\}$ denotes the probability operator; $|\cdot|$ denotes the absolute value operator; T denotes the time duration; $X(t|\mathrm{F}_{\mathrm{W}})$ denotes the system response of concern, corresponding to F_{W}; δ denotes the given threshold that limits the bounds of the safe domain.

In most engineering cases, the means and standard deviations of the system responses have received more attention. Based on the property presented in Eq. (4), the means and standard deviations of $\mathrm{X}^{\mathrm{P.B.}}(t)$ can serve as intervals and be denoted as follows:

$$\begin{cases} \mu_{\mathrm{X}}^{\mathrm{I}}(t) = \left[\mu_{\mathrm{X}}^{\mathrm{L}}(t), \mu_{\mathrm{X}}^{\mathrm{U}}(t)\right] \\ \sigma_{\mathrm{X}}^{\mathrm{I}}(t) = \left[\sigma_{\mathrm{X}}^{\mathrm{L}}(t), \sigma_{\mathrm{X}}^{\mathrm{U}}(t)\right] \end{cases} \tag{10}$$

Therefore, another objective of the UP analysis involves calculating the lower and upper bounds of the mean and standard deviation of the responses,[57] i.e., $\mu_{\mathrm{X}}^{\mathrm{L}}(t)$, $\mu_{\mathrm{X}}^{\mathrm{U}}(t)$, $\sigma_{\mathrm{X}}^{\mathrm{L}}(t)$, and $\sigma_{\mathrm{X}}^{\mathrm{U}}(t)$. Because the means and standard deviations of the responses are always dependent, the error bars[58] can be used to evaluate the overall uncertain extent of the responses. The lower-and-upper-bound intervals of the error bars, i.e., $\mathrm{e}_{\mathrm{L}}^{\mathrm{I}}$ and $\mathrm{e}_{\mathrm{U}}^{\mathrm{I}}$, for P-box problems, can be expressed as follows:

$$\begin{cases} \mathrm{e}_{\mathrm{L}}^{\mathrm{I}}(t) = \mu_{\mathrm{X}}^{\mathrm{I}}(t) - \sigma_{\mathrm{X}}^{\mathrm{I}}(t) \\ \mathrm{e}_{\mathrm{U}}^{\mathrm{I}}(t) = \mu_{\mathrm{X}}^{\mathrm{I}}(t) + \sigma_{\mathrm{X}}^{\mathrm{I}}(t) \end{cases} \tag{11}$$

The minimum value of the lower bounds $\mathrm{e}_{\mathrm{L}}^{\mathrm{L}}$ and the maximum value of the upper bounds $\mathrm{e}_{\mathrm{U}}^{\mathrm{U}}$ can be selected to quantify the error bars as follows:

$$\begin{cases} \mathrm{e}_{\mathrm{L}}^{\mathrm{L}}(t) = \min\limits_{\mathrm{F}_{\mathrm{W}} \in \left[\mathrm{F}_{\mathrm{W}}^{\mathrm{L}}, \mathrm{F}_{\mathrm{W}}^{\mathrm{U}}\right]} \mathrm{e}_{\mathrm{L}}^{\mathrm{I}}(t|\mathrm{F}_{\mathrm{W}}) \\ \mathrm{e}_{\mathrm{U}}^{\mathrm{U}}(t) = \max\limits_{\mathrm{F}_{\mathrm{W}} \in \left[\mathrm{F}_{\mathrm{W}}^{\mathrm{L}}, \mathrm{F}_{\mathrm{W}}^{\mathrm{U}}\right]} \mathrm{e}_{\mathrm{U}}^{\mathrm{I}}(t|\mathrm{F}_{\mathrm{W}}) \end{cases} \tag{12}$$

The essence of the problems presented in Eq. (8), Eq. (9), and Eq. (12) is to find the realizations that result in the bounds of the probabilistic characteristics of the system responses, within the given P-boxes $[\mathrm{F}_{\mathrm{W}}^{\mathrm{L}}, \mathrm{F}_{\mathrm{W}}^{\mathrm{U}}]$.

In some studies, these realizations for linear systems are searched by using an optimization technique.[50] However, for nonlinear dynamics, the methods based on optimizations have the following shortages. First, finding the global optimum is difficult, especially, when the stochastic analysis of nonlinear systems is complex. Second, the optimization has to be performed at many (even all) time nodes within the entire time span. Third, for multi-dimensional P-box processes, constructing the optimization problem has been shown to be difficult. Therefore, there is an urgent need to obtain an efficient method to achieve the UP analysis of nonlinear dynamics with distribution-free P-box processes.

3. Proposed method

In this section, a novel method is proposed to efficiently analyze the UP problems presented in Section 2.2, based on the

Please cite this article in press as: ZHANG L et al. An efficient uncertainty propagation method for nonlinear dynamics with distribution-free P-box processes, *Chin J Aeronaut* (2024), https://doi.org/10.1016/j.cja.2024.05.028

CADET and the Chebyshev method, which will be introduced in the following subsections.

3.1. Transcription of P-box dynamics using CADET

First, the P-box problem presented in Eq. (7) is transformed into an interval problem by using the CADET.

In the CADET, the nonlinear function $\mathrm{f}(\cdot)$ of the stochastic system presented in Eq. (1) is approximated by using the linear equation based on the statistical linearization:[59]

$$\mathrm{f}(\mathrm{X},t) \approx \mathrm{N}_{\mu}\mu_{\mathrm{X}} + \mathrm{N}_{R}\mathrm{R} \tag{13}$$

where μ_{X} denotes the N-dimensional mean vector of $\boldsymbol{X}$, i.e., $\mu_{\mathrm{X}} = E(\mathrm{X})$, $\boldsymbol{R}$ denotes the N-dimensional random-part vector of $\boldsymbol{X}$, i.e., $\mathrm{R} = \mathrm{X} - \mu_{\mathrm{X}}$, and N_{μ} and N_{R} represent the corresponding N by N real linear-coefficient matrices. In a probabilistic sense, the optimal N_{μ} and N_{R} that provide a minimum variance approximation can be, respectively, expressed as follows:[60]

$$\begin{cases} \mathrm{N}_{\mu}\mu_{\mathrm{X}} = \int_{-\infty}^{\infty} \mathrm{f}(\mathrm{x},t)d(\mathrm{F}_{\mathrm{X}}(\mathrm{x})) \\ \mathrm{N}_{R} = \int_{-\infty}^{\infty} \mathrm{f}(\mathrm{x},t)\mathrm{R}^{\mathrm{T}}d(\mathrm{F}_{\mathrm{X}}(\mathrm{x}))\cdot \mathrm{P}_{\mathrm{X}}^{-1} \end{cases} \tag{14}$$

where P_{X} denotes the N by N covariance matrix of $\boldsymbol{X}$, i.e., $\mathrm{P}_{\mathrm{X}} = E(\mathrm{R}\mathrm{R}^{\mathrm{T}})$, and $\mathrm{F}_{\mathrm{X}}(\cdot)$ denotes the joint CDF of $\boldsymbol{X}$. Subsequently, when the excitation $\mathrm{W}(t)$ consists of white noise processes, the nonlinear Ordinary Differential Equations (ODEs) governing the propagation of the mean vector μ_{X} and covariance matrix P_{X} for the system responses can be established as follows:[59]

$$\begin{cases} \dot{\mu}_{\mathrm{X}} = \mathrm{N}_{\mu}\mu_{\mathrm{X}} + \mathrm{B}\mu_{\mathrm{W}} \\ \dot{\mathrm{P}}_{\mathrm{X}} = \mathrm{N}_{R}\mathrm{P}_{\mathrm{X}} + \mathrm{P}_{\mathrm{X}}\mathrm{N}_{R} + \mathrm{B}\mathrm{P}_{\mathrm{W}}\mathrm{B}^{\mathrm{T}} \end{cases} \tag{15}$$

where μ_{W} denotes the mean vector of the excitations, i.e., $\mu_{\mathrm{W}} = E(\mathrm{W})$, and P_{W} denotes the covariance matrix of the excitations, i.e., $\mathrm{P}_{\mathrm{W}} = E[(\mathrm{W}-\mu_{\mathrm{W}})(\mathrm{W}-\mu_{\mathrm{W}})^{\mathrm{T}}]$. Of note, because the joint CDF of $\boldsymbol{X}$ in Eq. (14), i.e., $\mathrm{F}_{\mathrm{X}}(\cdot)$, for calculating N_{μ} and N_{R} is unknown, the ODEs in Eq. (15) cannot be solved directly. To address this issue, a crucial Gaussian assumption,[59] i.e., the responses are previously assumed to be jointly normal, is introduced. This Gaussian assumption follows from the central limit theorem and has been verified to be valid in practice.[60] Based on this assumption, $\mathrm{F}_{\mathrm{X}}(\cdot)$ can be described by using only its mean vector μ_{X} and covariance matrix P_{X}:

$$\mathrm{F}_{\mathrm{X}}(\mathrm{x},t) \approx \Phi_{\mathrm{X}}(\mathrm{x},t|\mu_{\mathrm{X}},\mathrm{P}_{\mathrm{X}}) \tag{16}$$

where $\Phi_{\mathrm{X}}(\cdot|\mu_{\mathrm{X}},\mathrm{P}_{\mathrm{X}})$ represents the normal distribution function with the mean vector μ_{X} and covariance matrix P_{X}. By substituting Eq. (16) into Eq. (14), $\mathrm{N}_{\mu}\mu_{\mathrm{X}}$ and N_{R} can both be described as functions of μ_{X} and P_{X}. After that, the ODEs in Eq. (15) can be fully defined as equations of μ_{X} and P_{X}. With the given initial values of μ_{X} and P_{X}, the ODEs can be solved by using any numerical method. The detailed method used to solve the CADET Eq. (15) is provided in the Ref. 59

For Eq. (7), according to the property expressed in Eq. (4), the components of the mean vector and covariance matrix of $\mathrm{W}^{\mathrm{P.B.}}(t)$ become intervals. The interval-valued mean vector and covariance matrix of $\mathrm{W}^{\mathrm{P.B.}}(t)$ are denoted as $\mu_{\mathrm{W}}^{\mathrm{I}}$ and $\mathrm{P}_{\mathrm{W}}^{\mathrm{I}}$, respectively. By substituting $\mu_{\mathrm{W}}^{\mathrm{I}}$ and $\mathrm{P}_{\mathrm{W}}^{\mathrm{I}}$ into Eq. (15), Eq. (15) can be transformed into ODEs under interval parameters:

$$\begin{cases} \dot{\mu}_{\mathrm{X}}^{\mathrm{I}} = \mathrm{N}_{\mu}^{\mathrm{I}}\mu_{\mathrm{X}}^{\mathrm{I}} + \mathrm{B}\mu_{\mathrm{W}}^{\mathrm{I}} \\ \dot{\mathrm{P}}_{\mathrm{X}}^{\mathrm{I}} = \mathrm{N}_{R}^{\mathrm{I}}\mathrm{P}_{\mathrm{X}}^{\mathrm{I}} + \mathrm{P}_{\mathrm{X}}^{\mathrm{I}}\mathrm{N}_{R}^{\mathrm{I}} + \mathrm{B}\mathrm{P}_{\mathrm{W}}^{\mathrm{I}}\mathrm{B}^{\mathrm{T}} \end{cases} \tag{17}$$

where $\mu_{\mathrm{X}}^{\mathrm{I}}$ and $\mathrm{P}_{\mathrm{X}}^{\mathrm{I}}$ denote the interval-valued mean vector and covariance matrix of the system responses, respectively, corresponding to $\mu_{\mathrm{W}}^{\mathrm{I}}$ and $\mathrm{P}_{\mathrm{W}}^{\mathrm{I}}$; $\mathrm{N}_{\mu}^{\mathrm{I}}$ and $\mathrm{N}_{R}^{\mathrm{I}}$ also become intervals as they are both functions of $\mu_{\mathrm{X}}^{\mathrm{I}}$ and $\mathrm{P}_{\mathrm{X}}^{\mathrm{I}}$.

Eq. (17) provides the interval bounds of the mean and variance of the system responses $\mathrm{X}^{\mathrm{P.B.}}(t)$, which are essential for achieving the UP analysis presented in Section 2.2. However, before solving Eq. (17), it is necessary to determine the bounds of the interval inputs, i.e., $\{\boldsymbol{\mu}_{W}^{\mathrm{I}}, \boldsymbol{P}_{W}^{\mathrm{I}}\}$. Meanwhile, an efficient algorithm is needed to solve the ODEs under these interval parameters. The methods for addressing these two issues will be introduced in Sections 3.2 and 3.3.

3.2. Domain analysis for mean and variance of the input P-box processes

In this subsection, the method for calculating $\{\boldsymbol{\mu}_{W}^{\mathrm{I}}, \boldsymbol{P}_{W}^{\mathrm{I}}\}$ is introduced. In this work, the stochastic excitations are assumed to be mutually independent. Therefore, $\mathrm{P}_{\mathrm{W}} = \mathrm{diag}(\sigma_{W_1}^2, \sigma_{W_2}^2, \ldots, \sigma_{W_M}^2)$, where $\sigma_{W_1}^2$, $\sigma_{W_2}^2$, …, and $\sigma_{W_M}^2$ represent the variances of the excitations. For simplicity, these variances are expressed as a vector $\sigma_{\mathrm{W}}^2 = [\sigma_{W_1}^2, \sigma_{W_2}^2, \ldots, \sigma_{W_M}^2]^{\mathrm{T}}$. For $\mathrm{W}^{\mathrm{P.B.}}(t)$, the values of its variance vector are intervals and can be denoted by $(\sigma_{\mathrm{W}}^2)^{\mathrm{I}}$. The calculation of $\{\boldsymbol{\mu}_{W}^{\mathrm{I}}, \boldsymbol{P}_{W}^{\mathrm{I}}\}$ is accordingly simplified to that of $\{\mu_{\mathrm{W}}^{\mathrm{I}}, (\sigma_{\mathrm{W}}^2)^{\mathrm{I}}\}$. For each component of $\mathrm{W}^{\mathrm{P.B.}}(t)$, i.e., $W_m^{\mathrm{P.B.}}(t)$ ($m = 1, 2, \ldots, M$), its bounds of the mean and variance are denoted by $\mu_{W_m}^{\mathrm{I}}$ and $(\sigma_{W_m}^2)^{\mathrm{I}}$, respectively. Because $W_m^{\mathrm{P.B.}}(t)$ is defined based on the given P-box $[F_{W_m}^{\mathrm{L}}, F_{W_m}^{\mathrm{U}}]$ using Eq. (3), $\mu_{W_m}^{\mathrm{I}}$ and $(\sigma_{W_m}^2)^{\mathrm{I}}$ can be calculated by substituting $[F_{W_m}^{\mathrm{L}}, F_{W_m}^{\mathrm{U}}]$ into Eq. (4), which can be expressed as follows:

$$\begin{cases} \mu_{W_m}^{\mathrm{I}} = \left[\min\limits_{F_{W_m}\in[F_{W_m}^{\mathrm{L}},F_{W_m}^{\mathrm{U}}]} \mathrm{mean}(F_{W_m}), \max\limits_{F_{W_m}\in[F_{W_m}^{\mathrm{L}},F_{W_m}^{\mathrm{U}}]} \mathrm{mean}(F_{W_m})\right] \\ (\sigma_{W_m}^2)^{\mathrm{I}} = \left[\min\limits_{F_{W_m}\in[F_{W_m}^{\mathrm{L}},F_{W_m}^{\mathrm{U}}]} var(F_{W_m}), \max\limits_{F_{W_m}\in[F_{W_m}^{\mathrm{L}},F_{W_m}^{\mathrm{U}}]} var(F_{W_m})\right] \end{cases} \tag{18}$$

The goal of solving the above minimization-and-maximization problems is to find the realizations that result in the bounds of its mean and variance within $[F_{W_m}^{\mathrm{L}}, F_{W_m}^{\mathrm{U}}]$. Therefore, introducing a method to generate CDF realizations of the P-box, is the primary work for solving the optimizations. In this work, a discretization-based method is used, which is described in the following subsections.

3.2.1. Generation of P-box realizations by discretization technique

To generate the CDF realizations of the P-box $[F_{W_m}^{\mathrm{L}}, F_{W_m}^{\mathrm{U}}]$, its support interval is equally discretized to obtain N_{s} grid points, denoted by $\boldsymbol{\omega}_{\mathrm{s}} = [\omega_1, \omega_2, \cdots, \omega_{N_s}]^{\mathrm{T}}$, as shown in Fig. 3. Then, an N_{s}-dimensional interval domain is obtained, as follows:

$$\mathrm{F}_{W_m}^{\mathrm{I}} = \left[F_{W_m}^{\mathrm{L}}(\omega_{\mathrm{s}}), F_{W_m}^{\mathrm{U}}(\omega_{\mathrm{s}})\right] \in \mathbb{IR}^{N_s} \tag{19}$$

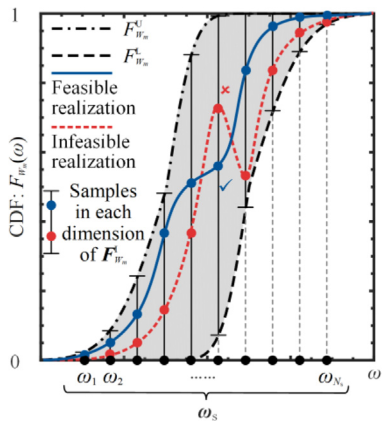

Fig. 3 Illustration of P-box discretization for the generation of realizations.

A set of samples is subsequently collected within $\mathrm{F}^{\mathrm{I}}_{W_m}$, denoted by $\mathrm{F}_{\mathrm{s}} \in \mathrm{F}^{\mathrm{I}}_{W_m}$, which contains N_{s} elements. Based on F_{s} and ω_{s}, a realization of $[F^{\mathrm{L}}_{W_m}, F^{\mathrm{U}}_{W_m}]$ and its inverse, denoted by $F_{W_m}(\omega)$ and $(F_{W_m})^{-1}(F)$, respectively, can be generated by the following interpolations:

$$\begin{cases} F_{W_m}(\omega) = \mathrm{interp}(\omega|\omega_{\mathrm{s}}, \mathrm{F}_{\mathrm{s}}) \\ (F_{W_m})^{-1}(F) = \mathrm{interp}(F|\mathrm{F}_{\mathrm{s}}, \omega_{\mathrm{s}}) \end{cases} \tag{20}$$

where $\mathrm{interp}(\cdot)$ denotes an interpolation operator. An example of the realization generation is illustrated in Fig. 3. It should be noted that if Eq. (21) is not satisfied, the sample vector F_{s} leads to an infeasible realization that is not monotonic, as shown in Fig. 3.

$$\mathrm{CF}_{\mathrm{s}} \leqslant \mathbf{0} \tag{21}$$

where

$$\mathrm{C} = \begin{bmatrix} 1 & -1 & 0 & \cdots & 0 \\ 0 & 1 & -1 & \ddots & \vdots \\ \vdots & \ddots & \ddots & \ddots & 0 \\ 0 & \cdots & 0 & 1 & -1 \end{bmatrix}_{((N_{\mathrm{s}}-1)\times N_{\mathrm{s}})} \tag{22}$$

Based on the above discretization, a continuous CDF realization is parameterized into N_{s} variables that satisfy Eq. (21) within $\mathrm{F}^{\mathrm{I}}_{W_m}$.

3.2.2. Domain analysis for mean and variance

According to the discretization procedure in Section 3.2.1, the optimizations presented in Eq. (18) can be transformed into optimization problems with N_{s} variables. For example, the minimization of the mean is expressed as follows:

$$\begin{aligned} &\min_{\mathrm{F}_{\mathrm{s}} \in \mathrm{F}^{\mathrm{I}}_{W_m}} \ \mathrm{mean}(F_{W_m}) \\ &\ \ \mathrm{s.t.} \ \ \mathrm{CF}_{\mathrm{s}} \leqslant \mathbf{0} \end{aligned} \tag{23}$$

These $N_{\mathrm{s}}-$dimensional optimizations can be easily solved. However, from Eq. (5), it is obvious that the calculations of mean and variance are not independent. As a result, the mean and variance cannot be minimized or maximized simultaneously. Specifically, several multi-objective problems need to be solved and can be expressed as follows:

$$\begin{cases} \min\limits_{\mathrm{F}_{\mathrm{s}} \in \mathrm{F}^{\mathrm{I}}_{W_m}} \ [\mathrm{mean}(F_{W_m}), var(F_{W_m})] \\ \min\limits_{\mathrm{F}_{\mathrm{s}} \in \mathrm{F}^{\mathrm{I}}_{W_m}} \ [-\mathrm{mean}(F_{W_m}), var(F_{W_m})] \\ \min\limits_{\mathrm{F}_{\mathrm{s}} \in \mathrm{F}^{\mathrm{I}}_{W_m}} \ [\mathrm{mean}(F_{W_m}), -var(F_{W_m})] \\ \min\limits_{\mathrm{F}_{\mathrm{s}} \in \mathrm{F}^{\mathrm{I}}_{W_m}} \ [-\mathrm{mean}(F_{W_m}), -var(F_{W_m})] \end{cases} \tag{24}$$
$$\mathrm{s.t.} \ \ \mathrm{CF}_{\mathrm{s}} \leqslant \mathbf{0}$$

The non-dominated solutions of these multi-objective problems will form the boundary of the 2-dimensional domain of mean and variance for a P-box. The interval box directly generated by $\mu^{\mathrm{I}}_{W_m} \otimes (\sigma^2_{W_m})^{\mathrm{I}}$, with $\otimes$ denoting the tensor product, is not the actual boundary. This will be validated and visualized in several cases at the end of this subsection.

These multi-objective optimizations can be solved by certain heuristic multi-objective optimization algorithms. However, to avoid the randomness of heuristic algorithms, a sampling-based approach is applied, in this work, to calculate the boundary of the domain of mean and variance. The uniformly distributed samples within $\mathrm{F}^{\mathrm{L}}_{W_m}$ are collected and the samples that do not satisfy Eq. (21) are removed. Then, the sample set is expressed as follows:

$$\{\mathrm{F}^{(k)}_{\mathrm{s}} | \mathrm{F}^{(k)}_{\mathrm{s}} \in \mathrm{F}^{\mathrm{I}}_{W_m}, \mathrm{CF}^{(k)}_{\mathrm{s}} \leqslant \mathbf{0}, k = 1, 2, \ldots, N_{\mathrm{R}_m}\} \tag{25}$$

where N_{R_m} denotes the number of feasible samples that satisfy Eq. (21). Based on $\mathrm{F}^{(k)}_{\mathrm{s}}$ ($k = 1, 2, \ldots, N_{\mathrm{R}_m}$), CDF realizations of the P-box can be generated by performing the interpolation presented in Eq. (20). Then, they are collected in the following set:

$$\left\{F^{(k)}_{W_m}(\omega) \middle| F^{(k)}_{W_m}(\omega) = \mathrm{interp}\left(\omega \middle| \omega_{\mathrm{s}}, \mathrm{F}^{(k)}_{\mathrm{s}}\right), k = 1, 2, \ldots, N_{\mathrm{R}_m}\right\} \tag{26}$$

For the kth realization $F^{(k)}_{W_m}(\cdot)$, the corresponding mean $\mu^{(k)}_{W_m}$ and variance $(\sigma^2_{W_m})^{(k)}$ can be calculated by the integration presented in Eq. (5), as follows:

$$\begin{cases} \mu^{(k)}_{W_m} = \int_{-\infty}^{\infty} \left(F^{(k)}_{W_m}\right)^{-1} \circ \Phi(\eta) d(\Phi(\eta)) \\ (\sigma^2_{W_m})^{(k)} = \int_{-\infty}^{\infty} \left(\left(F^{(k)}_{W_m}\right)^{-1} \circ \Phi(\eta) - \mu^{(k)}_{W_m}\right)^2 d(\Phi(\eta)) \end{cases} \tag{27}$$

where η denotes the integration variable. By calculating Eq. (27) from $k = 1$ to N_{R_m}, the sample set of the mean and variance of $W^{\mathrm{P.B.}}_m(t)$, denoted by C_{W_m}, can be obtained as follows:

$$\mathrm{C}_{W_m} = \left\{\mu^{(k)}_{W_m}, (\sigma^2_{W_m})^{(k)} | k = 1, 2, \ldots, N_{\mathrm{R}_m}\right\}, \quad m = 1, 2, \ldots, M \tag{28}$$

The interval bounds, i.e., $\mu^{\mathrm{I}}_{W_m} = [\mu^{\mathrm{L}}_{W_m}, \mu^{\mathrm{U}}_{W_m}]$ and $(\sigma^2_{W_m})^{\mathrm{I}} = [(\sigma^2_{W_m})^{\mathrm{L}}, (\sigma^2_{W_m})^{\mathrm{U}}]$, can also be easily determined by finding the minimum and maximum of the mean and variance, respectively, within these samples. Accordingly, the interval domain $\mu^{\mathrm{I}}_{W_m} \otimes (\sigma^2_{W_m})^{\mathrm{I}}$, denoted by I_{W_m}, is also obtained. The entire procedure for constructing C_{W_m} and I_{W_m} is illustrated in Fig. 4.

By applying the above procedure to the M P-box processes, the domains I_{W_m} and C_{W_m} ($m = 1, 2, \ldots, M$) are obtained. Then, the entire hypercube interval domain of the M means and M variances is constructed as follows:

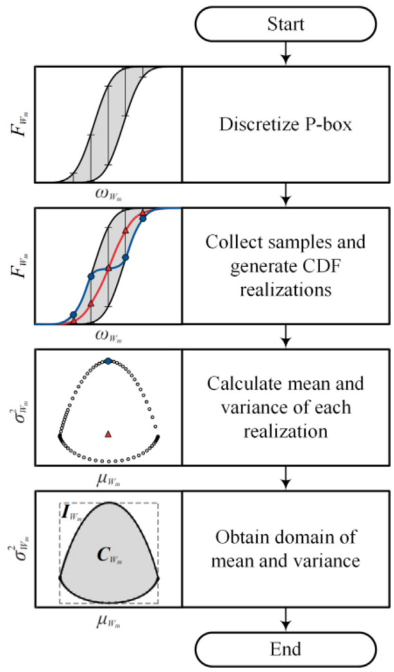

Fig. 4 Flowchart of domain analysis for mean and variance.

$$\mathrm{I_W} = \mathrm{I}_{W_1} \otimes \mathrm{I}_{W_2} \otimes \cdots \otimes \mathrm{I}_{W_M} \in \mathbb{IR}^{2M} \tag{29}$$

The complete sample set of M means and M variances are constructed by the orthogonal combinations of the samples in C_{W_m} $(m = 1, 2, \ldots, M)$ as follows:

$$\begin{aligned} &\mathrm{C_W} = \mathrm{C}_{W_1} \otimes \mathrm{C}_{W_2} \otimes \cdots \otimes \mathrm{C}_{W_M} \\ &= \left\{ \mu_{\mathrm{Ws}}^{(k)}, \left(\sigma_{\mathrm{Ws}}^2\right)^{(k)} | k = 1, 2, \ldots, N_{\mathrm{C}} \right\} \end{aligned} \tag{30}$$

where

$$\begin{cases} \mu_{\mathrm{Ws}}^{(k)} = \left[\mu_{W_1}^{(k)}, \mu_{W_2}^{(k)}, \ldots, \mu_{W_M}^{(k)}\right]^{\mathrm{T}} \\ \left(\sigma_{\mathrm{Ws}}^2\right)^{(k)} = \left[\left(\sigma_{W_1}^2\right)^{(k)}, \left(\sigma_{W_2}^2\right)^{(k)}, \ldots, \left(\sigma_{W_M}^2\right)^{(k)}\right]^{\mathrm{T}} \\ N_{\mathrm{C}} = N_{R_1} \times N_{R_2} \ldots \times N_{R_M} \end{cases} \tag{31}$$

where $\mu_{\mathrm{Ws}}^{(k)}$ and $\left(\sigma_{\mathrm{Ws}}^2\right)^{(k)}$ denote the vectors consisting of the kth set of samples of M means and variances, respectively; their mth $(m = 1, 2, \ldots, M)$ component, i.e., $\mu_{W_m}^{(k)}$ and $\left(\sigma_{W_m}^2\right)^{(k)}$, is from C_{W_m} as presented in Eq. (28); N_{C} denotes the total number of the samples within $\mathrm{C_W}$, and N_{R_m} is the sample number of C_{W_m}.

To demonstrate the domains of the mean and variance intuitively, four representative cases of the distribution-free P-box are collected and summarized in Table 1, with $W_1^{\mathrm{P.B.}}$, $W_2^{\mathrm{P.B.}}$, and $W_3^{\mathrm{P.B.}}$ obtained from the literature.[50] The corresponding P-boxes are presented in Fig. 5(a), Fig. 6(a), Fig. 7(a), and Fig. 8(a). These P-boxes are discretized into 500 slices, i.e., $N_{\mathrm{s}} = 500$, and 3 uniformly distributed samples are collected in each dimension. Then, the corresponding domains are presented in Fig. 5(b), Fig. 6(b), Fig. 7(b), and Fig. 8(b). As mentioned above, the actual domain of the mean and variance, i.e., C_{W_m}, is a convex subset of the hypercube I_{W_m}, which is due to the interdependence between the mean and variance. Accordingly, the uncertain ODEs presented in Eq. (17) have to be solved based on the convex set C_{W_m}, and the method for solving this problem will be introduced in the following subsection.

Table 1 Cases of P-box,[50] where B, N, W, and EXP represent the beta, normal, Weibull, and exponential distributions, respectively.

Case	Symbol	$F_W^{\mathrm{L}}(\omega)$	$F_W^{\mathrm{U}}(\omega)$
1	$W_1^{\mathrm{P.B.}}$	min [B(1, 1), B(2, 5)]	max [B(1, 1), B(2, 5)]
2	$W_2^{\mathrm{P.B.}}$	min [B(1, 0.2), B(5, 5)]	max [B(1, 0.2), B(5, 5)]
3	$W_3^{\mathrm{P.B.}}$	min [N(0, 0.75), B(1, 0.2)]	max [N(0, 0.75), B(1, 0.2)]
4	$W_4^{\mathrm{P.B.}}$	min [W(0.1, 0.6), EXP (0.5)]	max [W(0.1, 0.6), EXP (0.5)]

3.3. Chebyshev-polynomial-based method for interval ODEs

After determining the domain of the means and variances of the excitations, the interval nonlinear ODEs presented in Eq. (17) are completely defined. The Chebyshev method[30] has been proven to perform well in solving nonlinear dynamics under interval uncertainties. Therefore, this method is applied and modified to solve the interval ODEs, addressing the irregular convex domain $\mathrm{C_W}$ presented in Eq. (30).

For notational convenience, $\{\mu_{\mathrm{X}}, \mathrm{P_X}\}$ is denoted by $\boldsymbol{y}$ and $\{\mu_{\mathrm{W}}, \mathrm{P_W}\}$ is denoted by $\boldsymbol{z}$. For mutually independent excitations, $\boldsymbol{z}$ represents $\{\mu_{\mathrm{W}}, \sigma_{\mathrm{W}}^2\} \in \mathbb{R}^{2M}$, which is a $2M$-dimensional vector including M means and M variances. Then, the solution of CADET equations (15) can be expressed as follows:

$$\mathrm{y(z}|t) = \{\mathrm{y}|\dot{\mathrm{y}} = \mathrm{f_{CADET}}(\mathrm{y}, \mathrm{z}, t)\} \tag{32}$$

where $\mathrm{f_{CADET}}(\cdot)$ denotes the vector function on the right-hand side of Eq. (15). $\mathrm{y(z}|t)$ can be regarded as the vector function with respect to $\boldsymbol{z}$. At a certain time instant t, any component of the vector function $\mathrm{y(z}|t)$, denoted by $y(\mathrm{z}|t) \in \mathrm{y(z}|t)$, can be approximated by using the Chebyshev polynomial, denoted by $p_{y(t)}(\mathrm{z})$, which can be generally expressed as follows:[30]

$$\begin{aligned} y(\mathrm{z}|t) \approx p_{y(t)}(\mathrm{z}) = \sum_{0 < i_1 + i_2 + \cdots + i_{2M} < d} c_{i_1, i_2, \ldots, i_{2M}} C_{i_1, i_2, \ldots, i_{2M}}(\boldsymbol{z}), \\ i_1,\ i_2,\ \ldots,\ i_{2M} = 0,\ 1,\ \ldots,\ d \end{aligned} \tag{33}$$

where d denotes the order of the Chebyshev polynomials, $C_{i_1, i_2, \ldots, i_{2M}}(\cdot)$ represents a $2M$-dimensional Chebyshev polynomial basis, as expressed in Eq. (34), and $c_{i_1, i_2, \ldots, i_{2M}}$ represents the corresponding coefficient of the polynomial.

$$C_{i_1, i_2, \ldots, i_{2M}}(\mathrm{z}) = \cos(i_1\theta_1)\cos(i_2\theta_2)\cdots\cos(i_{2M}\theta_{2M}) \tag{34}$$

where $[\theta_1,\ \theta_2,\ \ldots,\ \theta_{2M}]^{\mathrm{T}}$, also denoted by θ, is transformed from $\boldsymbol{z}$ with a given range $[\mathrm{z^L},\ \mathrm{z^U}]$ as follows:

$$\theta = \arccos\left(\frac{2\mathrm{z} - (\mathrm{z^L} + \mathrm{z^U})}{\mathrm{z^U} - \mathrm{z^L}}\right) \tag{35}$$

As discussed in Section 3.2.2, for Eq. (17), $[\mathrm{z^L},\ \mathrm{z^U}]$ has been determined as $\mathrm{I_W}$ presented in Eq. (29). Then, the coefficients $c_{i_1, i_2, \ldots, i_{2M}}$ can be determined by using the Chebyshev Collocation Method (CCM). The details regarding CCM are discussed

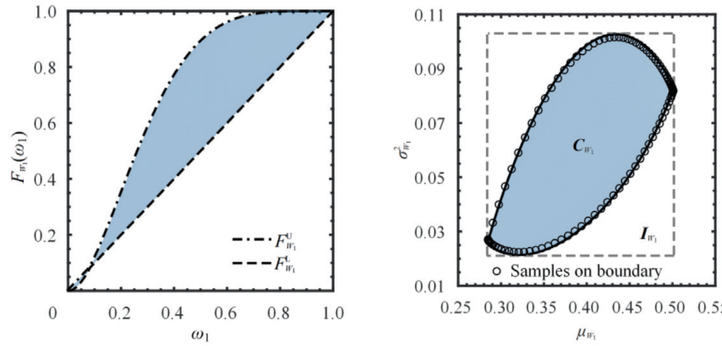

(a) P-box (b) Domain of $\mu\ W_1$ and $\sigma 2\ W_1$

Fig. 5 Case 1 of P-box and corresponding domains of mean and variance.

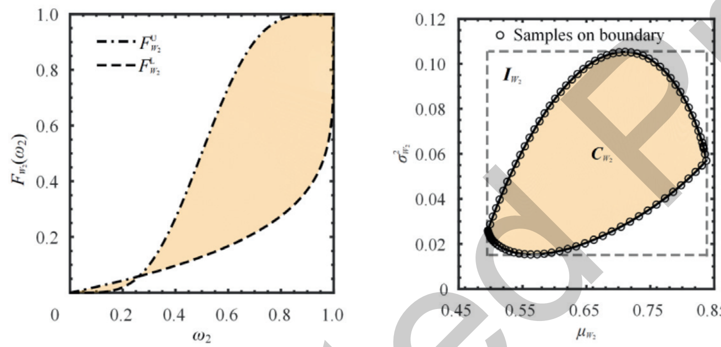

(a) P-box (b) Domain of $\mu\ W_2$ and $\sigma 2\ W_2$

Fig. 6 Case 2 of P-box and corresponding domains of mean and variance.

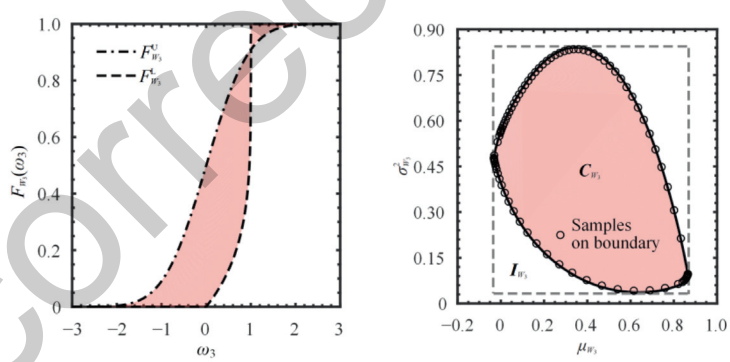

(a) P-box (b) Domain of $\mu\ W_3$ and $\sigma 2\ W_3$

Fig. 7 Case 3 of P-box and corresponding domains of mean and variance.

in the literature.[61] To use CCM, the N_p interpolation points of $\boldsymbol{z}$ need to be selected within the hypercube domain I_W as follows:

$$\left\{ \text{z}_\text{p}^{(k)} \in \text{I}_\text{W} \middle| k = 1, 2, \ldots, N_\text{p} \right\} \tag{36}$$

where $\text{z}_\text{p}^{(k)}$ denotes the kth set of interpolation points of $\boldsymbol{z}$. As discussed in the literature,[61] the interpolation point number N_p can be determined as follows:

$$N_\text{p} = \frac{2(2M+d)!}{(2M)!d!} \tag{37}$$

The procedure for collecting N_p interpolation points using CCM is also detailed in the literature.[61] Then, at each set of interpolation points presented in Eq. (36), the ODEs presented in Eq. (15) can be solved, which can be expressed as follows:

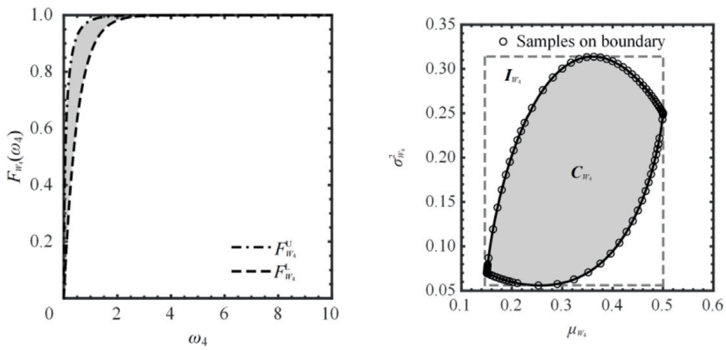

(a) P-box (b) Domain of μ W_4 and σ2 W_4

Fig. 8 Case 4 of P-box and corresponding domains of mean and variance.

$$\begin{cases} \mathrm{y}_{\mathrm{p}}^{(1)}(t) = \left\{ \mathrm{y}_{\mathrm{p}}^{(1)} \middle| \dot{\mathrm{y}}_{\mathrm{p}}^{(1)} = \mathrm{f}_{\mathrm{CADET}}\left(\mathrm{y}_{\mathrm{p}}^{(1)}, \mathrm{z}_{\mathrm{p}}^{(1)}, t\right) \right\} \\ \mathrm{y}_{\mathrm{p}}^{(2)}(t) = \left\{ \mathrm{y}_{\mathrm{p}}^{(2)} \middle| \dot{\mathrm{y}}_{\mathrm{p}}^{(2)} = \mathrm{f}_{\mathrm{CADET}}\left(\mathrm{y}_{\mathrm{p}}^{(2)}, \mathrm{z}_{\mathrm{p}}^{(2)}, t\right) \right\} \\ \vdots \\ \mathrm{y}_{\mathrm{p}}^{(N_{\mathrm{p}})}(t) = \left\{ \mathrm{y}_{\mathrm{p}}^{(N_{\mathrm{p}})} \middle| \dot{\mathrm{y}}_{\mathrm{p}}^{(N_{\mathrm{p}})} = \mathrm{f}_{\mathrm{CADET}}\left(\mathrm{y}_{\mathrm{p}}^{(N_{\mathrm{p}})}, \mathrm{z}_{\mathrm{p}}^{(N_{\mathrm{p}})}, t\right) \right\} \end{cases} \tag{38}$$

where $\mathrm{y}_{\mathrm{p}}^{(k)}(t)$ (k = 1, 2, …, N_{p}) denotes the solved interpolation samples of $\boldsymbol{y}$ corresponding to $\mathrm{z}_{\mathrm{p}}^{(k)}$ at time instant t, with the component denoted by $y_{\mathrm{p}}^{(k)}(t) \in \mathrm{y}_{\mathrm{p}}^{(k)}(t)$. Based on $y_{\mathrm{p}}^{(k)}(t)$ and $\mathrm{z}_{\mathrm{p}}^{(k)}$ (k = 1, 2, …, N_{p}), the polynomial coefficient $c_{i_1,i_2,\ldots,i_{2M}}$ presented in Eq. (33) can be determined using CCM. Then, the Chebyshev-polynomial approximation $p_{y(t)}(\mathrm{z})$ is constructed.

Based on $p_{y(t)}(\mathrm{z})$, the value of $y(t)$ corresponding to any given $\boldsymbol{z}$ can be calculated without calling the CADET equations. As discussed in Section 3.2.2, $\boldsymbol{z}$ $(=\{\mu_{\mathrm{W}}, \sigma^2_{\mathrm{W}}\})$ are enveloped in a convex set $\mathrm{C_W}$, and the samples of $\boldsymbol{z}$ within $\mathrm{C_W}$ have been generated as presented in Eq. (30). The values of $y(t)$ corresponding to all samples of $\boldsymbol{z}$ collected in $\mathrm{C_W}$, can be calculated by using $p_{y(t)}(\mathrm{z})$. Subsequently, the bounds, denoted by $y^{\mathrm{I}}(t)$, can be obtained by finding the minimums and maximums. This is the so-called scanning method, which can be expressed as follows:

$$y^{\mathrm{I}}(t) = \left[\min_{k=1,2,\ldots,N_{\mathrm{C}}} p_{y(t)}\left(\left\{\mu_{\mathrm{Ws}}^{(k)}, \left(\sigma^2_{\mathrm{Ws}}\right)^{(k)}\right\}\right), \max_{k=1,2,\ldots,N_{\mathrm{C}}} p_{y(t)}\left(\left\{\mu_{\mathrm{Ws}}^{(k)}, \left(\sigma^2_{\mathrm{Ws}}\right)^{(k)}\right\}\right) \right] \tag{39}$$

where $\{\mu_{\mathrm{Ws}}^{(k)}, (\sigma^2_{\mathrm{Ws}})^{(k)}\}$ is the kth set of samples within $\mathrm{C_W}$, and N_{C} is the total sample number of $\mathrm{C_W}$, as presented in Eq. (30) and Eq. (31).

Because $y(t)$ can represent any component of $\mathrm{y}(t)$ $(=\{\mu_{\mathrm{X}}(t), \mathrm{P_X}(t)\})$, the bounds of $\{\mu^{\mathrm{I}}_{\mathrm{X}}(t), \mathrm{P}^{\mathrm{I}}_{\mathrm{X}}(t)\}$ can be obtained by performing the procedure outlined from Eq. (33) to Eq. (39) for each component of $\{\mu_{\mathrm{X}}(t), \mathrm{P_X}(t)\}$. Of note, Eq. (38) only needs to be solved once to generate interpolation samples for all components of $\mu_{\mathrm{X}}(t)$ and $\mathrm{P_X}(t)$. Therefore, the number of solving the CADET function is only equal to the number of interpolation points N_{p} presented in Eq. (37).

3.4. Uncertainty propagation and a P-box Gaussian assumption

Because the bounds of $\mu^{\mathrm{I}}_{\mathrm{X}}(t)$ and $\mathrm{P}^{\mathrm{I}}_{\mathrm{X}}(t)$ have been obtained, the bounds of error bars, at time instant t, can be easily determined as follows:

$$\begin{cases} \mathrm{e}^{\mathrm{L}}_{\mathrm{L}}(t) = \min\limits_{\mu_{\mathrm{X}}, \mathrm{P_X} \in \left\{\mu^{\mathrm{I}}_{\mathrm{X}}(t), \mathrm{P}^{\mathrm{I}}_{\mathrm{X}}(t)\right\}} \left(\mu_{\mathrm{X}} - \sqrt{\mathrm{diag}(\mathrm{P_X})}\right) \\ \mathrm{e}^{\mathrm{U}}_{\mathrm{U}}(t) = \max\limits_{\mu_{\mathrm{X}}, \mathrm{P_X} \in \left\{\mu^{\mathrm{I}}_{\mathrm{X}}(t), \mathrm{P}^{\mathrm{I}}_{\mathrm{X}}(t)\right\}} \left(\mu_{\mathrm{X}} + \sqrt{\mathrm{diag}(\mathrm{P_X})}\right) \end{cases} \tag{40}$$

As discussed in Section 3.1, when solving the basic CADET in Eq. (15), the Gaussian assumption presented in Eq. (16) is utilized. This assumption is also meaningful for evaluating the CDF bounds of system responses $\mathrm{X}^{\mathrm{P.B.}}(t)$. Because the responses are assumed to be Gaussian processes, their distribution function is quantified based on μ_{X} and $\mathrm{P_X}$. When $\mu^{\mathrm{I}}_{\mathrm{X}}$ and $\mathrm{P}^{\mathrm{I}}_{\mathrm{X}}$ are interval values, at any time instant t, the distribution of $\mathrm{X}^{\mathrm{P.B.}}(t)$ is normal but the mean and variance are intervals. Hence, $\mathrm{X}^{\mathrm{P.B.}}(t)$ can be characterized as time-varying parametric Gaussian P-boxes, also referred to as parametric Gaussian P-box processes. Therefore, the Gaussian assumption for basic CADET can be extended to the P-box form. Regardless of the distribution-free P-box processes of excitation $\mathrm{W}^{\mathrm{P.B.}}(t)$, the system responses $\mathrm{X}^{\mathrm{P.B.}}(t)$ can be approximated by the parametric Gaussian P-box processes. This can be expressed mathematically as follows:

$$\begin{cases} \mathrm{F}^{\mathrm{L}}_{\mathrm{X}}(\mathrm{x}, t) \approx \min\limits_{\mu_{\mathrm{X}}, \mathrm{P_X} \in \left\{\mu^{\mathrm{I}}_{\mathrm{X}}(t), \mathrm{P}^{\mathrm{I}}_{\mathrm{X}}(t)\right\}} \Phi_{\mathrm{X}}(\mathrm{x}, t | \mu_{\mathrm{X}}, \mathrm{P_X}) \\ \mathrm{F}^{\mathrm{U}}_{\mathrm{X}}(\mathrm{x}, t) \approx \max\limits_{\mu_{\mathrm{X}}, \mathrm{P_X} \in \left\{\mu^{\mathrm{I}}_{\mathrm{X}}(t), \mathrm{P}^{\mathrm{I}}_{\mathrm{X}}(t)\right\}} \Phi_{\mathrm{X}}(\mathrm{x}, t | \mu_{\mathrm{X}}, \mathrm{P_X}) \end{cases} \tag{41}$$

The P-box Gaussian assumption and the CADET method have the same applicable conditions for nonlinear systems. Based on Eq. (41), it is possible to evaluate the CDF bounds of the responses.

Notably, although the proposed method can provide both the CDF bounds and error-bar bounds of the system responses, its main task is to calculate the error-bar bounds. The bounds of the first-passage probability presented in Eq. (9) cannot be determined as the auto-correlations of system responses, which are essential for the evaluation of the first-passage probability, cannot be provided by the CADET method. This issue deserves further investigation in the future.

Please cite this article in press as: ZHANG L et al. An efficient uncertainty propagation method for nonlinear dynamics with distribution-free P-box processes, *Chin J Aeronaut* (2024), https://doi.org/10.1016/j.cja.2024.05.028

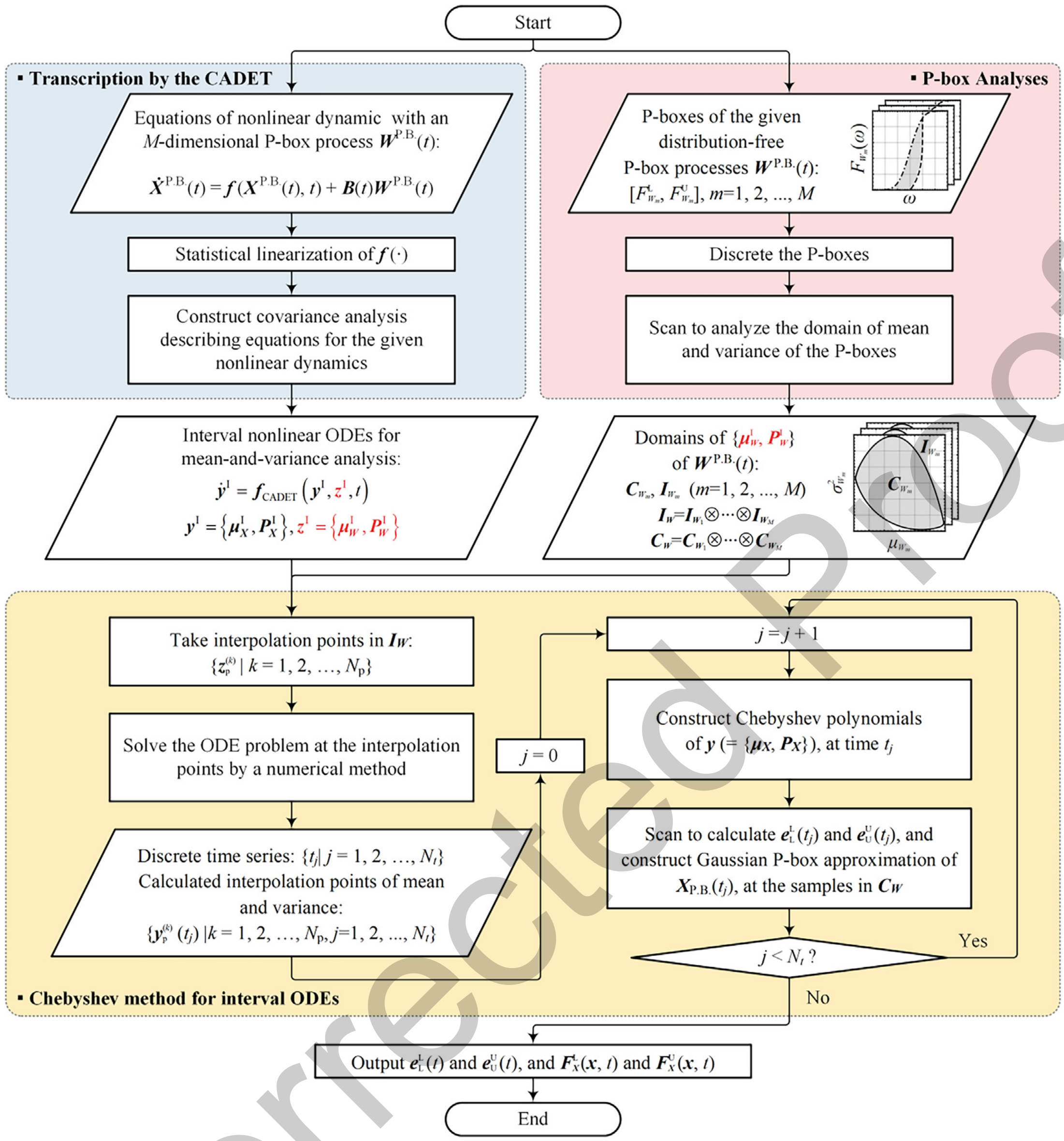

Fig. 9 Flowchart of the proposed uncertainty propagation method.

3.5. Entire procedure of proposed method

Based on the aforementioned approaches, it is possible to efficiently solve the nonlinear dynamics with distribution-free P-box processes. The entire procedure is concluded in the this subsection, with the corresponding flowchart presented in Fig. 9.

Step 1. Problem definition: As discussed in section 2, the nonlinear dynamical system with the $M-$dimensional $\mathrm{W}^{\mathrm{P.B.}}(t)$ is defined as Eq. (7). $\mathrm{W}^{\mathrm{P.B.}}(t)$ is defined by the M static P-boxes, denoted as $[\mathrm{F}_{\mathrm{W}}^{\mathrm{L}},\ \mathrm{F}_{\mathrm{W}}^{\mathrm{U}}]$, based on Eq. (3). The corresponding UP problems are defined as Eq. (8) and Eq. (12).

Step 2. Problem transcription by the CADET: As discussed in Section 3.1, the CADET equations, involving interval parameters $\{\mu_{\mathrm{W}}^{\mathrm{I}},\ \mathrm{P}_{\mathrm{W}}^{\mathrm{I}}\}$, are established as presented in Eq. (17). Therefore, the original P-box problem stated in Eq. (7) has been transformed into the corresponding interval problem as given by Eq. (17).

Step 3. Domain analysis of $\{\mu_{\mathrm{W}}^{\mathrm{I}},\ \mathrm{P}_{\mathrm{W}}^{\mathrm{I}}\}$: As discussed in subsection 3.2, the domain of $\{\mu_{\mathrm{W}}^{\mathrm{I}},\ \mathrm{P}_{\mathrm{W}}^{\mathrm{I}}\}$ is analyzed, by the following steps.

(1) As discussed in subsection 3.2.2, the CDF realization set of $[\mathrm{F}_{\mathrm{W}}^{\mathrm{L}},\ \mathrm{F}_{\mathrm{W}}^{\mathrm{U}}]$ is generated using the discretization technique, which is denoted as $\{F_{W_m}^{(k)}(\cdot)|k=1,2,\ldots,N_{\mathrm{R}_m}\}$ $(m = 1, 2, \ldots, M)$ and presented in Eq. (26) in detail.

(2) The means and variances corresponding to each $F_{W_m}^{(k)}(\cdot)$ are calculated by the integration presented in Eq. (27), from $k = 1$ to N_{R_m} and $m = 1$ to M. Then, the convex sample set $\mathrm{C_W}$ presented in Eq. (30) and the corresponding hypercube $\mathrm{I_W}$ presented in Eq. (29) are constructed.

Step 4. Chebyshev method for solving interval ODEs: The numerical ODE method and the corresponding discrete time series $\{t_j | j = 1, 2, \ldots, N_t\}$ are defined, and $j = 1$. $\{\mu_{\mathrm{X}}, \mathrm{P}_{\mathrm{X}}\}$ and $\{\mu_{\mathrm{W}}, \sigma^2_{\mathrm{W}}\}$ are collect in the vectors, denoted as $\boldsymbol{y}$ and $\boldsymbol{z}$, respectively.

(1) As discussed in subsection 3.3, the order of Chebyshev polynomial d is defined, and the required number of interpolation points N_{p} is determined by using Eq. (37). The N_{p} sets of interpolation points of $\boldsymbol{z}$, denoted as $\{\mathrm{z}_{\mathrm{p}}^{(k)} | k = 1, 2, \ldots, N_{\mathrm{p}}\}$, are obtained by using the CCM within the hypercube $\mathrm{I_W}$, as presented in Eq. (36).
(2) The CADET equations corresponding to $\mathrm{z}_{\mathrm{p}}^{(k)}$, presented in Eq. (38), are solved by the numerical method. Then, the corresponding N_{p} sets of interpolation samples of $\boldsymbol{y}$ at each discrete time instant, denoted by $\{\mathrm{y}_{\mathrm{p}}^{(k)}(t_j) | j = 1,\ 2,\ \ldots,\ N_t,\ k = 1,\ 2,\ \ldots,\ N_{\mathrm{p}}\}$, are obtained.
(3) At time instant t_j, the Chebyshev-polynomial approximations of each component of $\boldsymbol{y}$, presented in Eq. (33), are constructed based on $\mathrm{z}_{\mathrm{p}}^{(k)}$ and $\mathrm{y}_{\mathrm{p}}^{(k)}(t_j)$ ($k = 1,\ 2,\ \ldots,\ N_{\mathrm{p}}$) by using the CCM.
(4) The values of $\boldsymbol{y}$ corresponding to all samples of $\boldsymbol{z}$ collected in $\mathrm{C_W}$, are calculated by using the Chebyshev-polynomial approximations. Subsequently, the bounds of $\{\mu_{\mathrm{X}}^{\mathrm{I}}(t_j), \mathrm{P}_{\mathrm{X}}^{\mathrm{I}}(t_j)\}$ are obtained based on Eq. (39).

Step 5. Uncertainty propagation: At time instant t_j, the bounds of error bars, denoted as $\mathrm{e}_{\mathrm{L}}^{\mathrm{L}}(t_j)$ and $\mathrm{e}_{\mathrm{U}}^{\mathrm{U}}(t_j)$, are found by Eq. (40). Then, the system responses $\mathrm{X}^{\mathrm{P.B.}}(t)$ are assumed to be parametric Gaussian P-box processes, and the CDF bounds of the system responses, denoted as $\mathrm{F}_{\mathrm{X}}^{\mathrm{L}}(x, t_j)$ and $\mathrm{F}_{\mathrm{X}}^{\mathrm{U}}(x, t_j)$, are approximated by Eq. (41). Let $j = j + 1$.

Step 6. If $j < N_t$, return to step 4.3, otherwise, $\mathrm{e}_{\mathrm{L}}^{\mathrm{L}}(t)$ and $\mathrm{e}_{\mathrm{U}}^{\mathrm{U}}(t)$, as well as $\mathrm{F}_{\mathrm{X}}^{\mathrm{L}}(x, t)$ and $\mathrm{F}_{\mathrm{X}}^{\mathrm{U}}(x, t)$, at each discrete instant t_j ($j = 1,\ 2,\ \ldots,\ N_t$), are outputted.

Notably, the precision of the proposed transformation is governed by the inherent nonlinearity of the system. Once the nonlinear system is determined, the precision of the transformation presented in Section 3.1 cannot be significantly improved. The required computational cost increases as the number of excitation dimensions M increases. Moreover, the CADET is established based on a precondition that excitations are white noise processes; therefore, the uncertainties of time correlation for the excitations are not considered. However, the method is still meaningful as white noise with imprecise distribution information has also been commonly used in practical engineering.

4. Tests and setup

In this section, two numerical tests and an engineering application are implemented to demonstrate the effectiveness of the proposed method. The Runge–Kutta (RK) method is used to solve the ODEs. The order of the Chebyshev polynomials d is defined as 2. In subsection 3.3.2, N_{s} has been set to 500.

To test the accuracy of the method, the reference solutions are obtained by using an MC-based approach. The CDF realizations of the P-box have been collected, as presented in Eq. (26). Then, for each realization, MC simulations are performed to calculate the corresponding CDF and statistical moments of the system response. Finally, the sets of CDF realizations and statistical-moment samples for the system response can be obtained, and the reference solutions of the CDF and error-bar bounds can also be found within these sets. The detailed procedure of the MC-based approach is provided in Appendix A. In the following test cases, 10000-time MC simulations are performed for each CDF realization.

All the computations are performed using a personal computer with 16 GB of RAM and an Intel(R) Core(TM) i7-9750H @ 2.60 GHz CPU.

The P-box-process excitations considered in these test cases will be defined based on the four basic P-box processes. These basic P-box processes are constructed based on the P-boxes presented in Table 1 of Section 3.2.2, i.e., $W_1^{\mathrm{P.B.}}$, $W_2^{\mathrm{P.B.}}$, $W_3^{\mathrm{P.B.}}$, and $W_4^{\mathrm{P.B.}}$, by using Eq. (3) as follows:

$$W_i^{\mathrm{P.B.}}(t) = \left[\left(F_{W_i}^{\mathrm{L}} \right)^{-1}, \left(F_{W_i}^{\mathrm{U}} \right)^{-1} \right]^{\circ} \Phi(N_0(t)), \quad i = 1, 2, 3, 4 \tag{42}$$

where the subscript i represents the case ID in Table 1, and $N_0(t)$ denotes a standard white Gaussian noise process. Therefore, the excitations, in the following test cases, are considered as white noise with imprecise distribution information. The example of one sample trajectory of $N_0(t)$, denoted by $n_0(t)$, is shown in Fig. 10(a). Based on $n_0(t)$, sample trajectories of these basic P-box processes are generated, which are denoted by $\omega_1(t)$, $\omega_2(t)$, $\omega_3(t)$, and $\omega_4(t)$, respectively, as shown in Fig. 10(b)–(e), respectively.

It should be noted that the P-box for constructing $W_4^{\mathrm{P.B.}}$, i.e., $[F_{W_4}^{\mathrm{L}}, F_{W_4}^{\mathrm{U}}]$, has skewed distributions. The skewness of $F_{W_4}^{\mathrm{U}}$ is greater than 4, which is set to test the Gaussian assumption.

4.1. Numerical tests

4.1.1. Duffing oscillator analysis

First, a single-degree-of-freedom duffing oscillator system is modeled as follows:

$$m\ddot{x}(t) + c\dot{x}(t) + k\left(x(t) + \varepsilon (x(t))^3 \right) = u(t) \tag{43}$$

where $\ddot{x}$, $\dot{x}$, and x denote the acceleration, velocity, and displacement of the system, respectively; $u(t)$ denote the excitation of the system. m is equal to 1 kg, c, k, and ε, are equal to 0.5π, $4\pi^2$, and 1, respectively. The initial condition is given as $[\dot{x}(t_0),\ x(t_0)]^{\mathrm{T}} = [0,\ 0]^{\mathrm{T}}$.

Under an uncertain excitation, $U^{\mathrm{P.B.}}(t)$ is described as a distribution-free P-box process, and the problem is expressed as follows:

$$\begin{cases} \dot{V}^{\mathrm{P.B.}}(t) = \frac{1}{m}\left[-cV^{\mathrm{P.B.}}(t) - k\left(X^{\mathrm{P.B.}}(t) + \varepsilon \left(X^{\mathrm{P.B.}}(t) \right)^3 \right) \right] + \frac{1}{m} U^{\mathrm{P.B.}}(t) \\ \dot{X}^{\mathrm{P.B.}}(t) = V^{\mathrm{P.B.}}(t) \end{cases} \tag{44}$$

where $V^{\mathrm{P.B.}}(t)$ and $X^{\mathrm{P.B.}}(t)$ denote the velocity and displacement described as P-box processes, respectively. Four cases of $U^{\mathrm{P.B.}}(t)$, as shown in Table 2, are produced based on the lin-

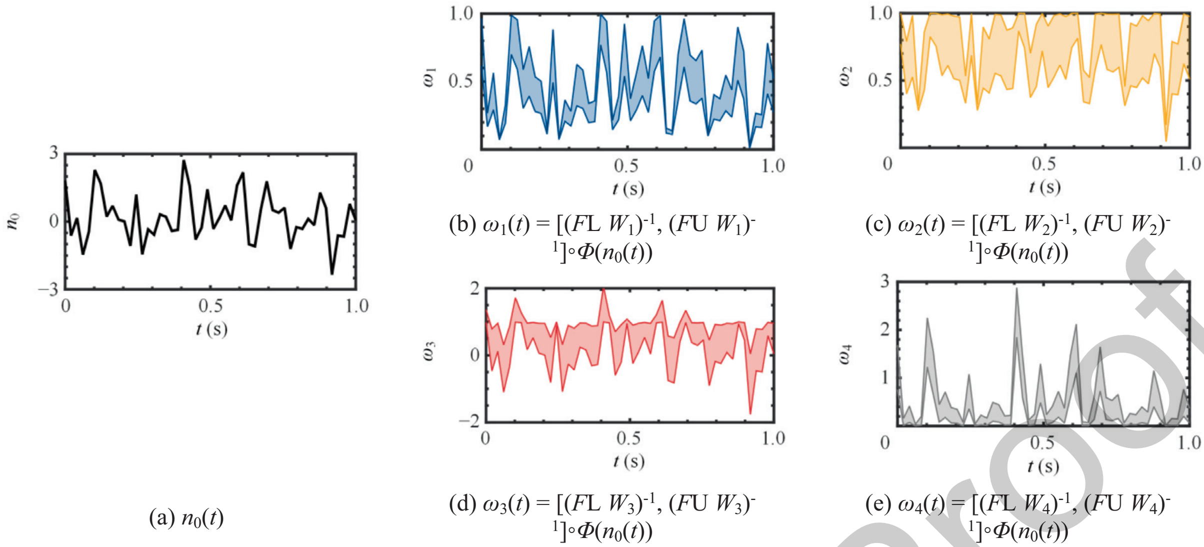

(a) $n_0(t)$

(b) $\omega_1(t) = [(FL\ W_1)^{-1}, (FU\ W_1)^{-1}]\circ\Phi(n_0(t))$

(c) $\omega_2(t) = [(FL\ W_2)^{-1}, (FU\ W_2)^{-1}]\circ\Phi(n_0(t))$

(d) $\omega_3(t) = [(FL\ W_3)^{-1}, (FU\ W_3)^{-1}]\circ\Phi(n_0(t))$

(e) $\omega_4(t) = [(FL\ W_4)^{-1}, (FU\ W_4)^{-1}]\circ\Phi(n_0(t))$

Fig. 10 One of the sample trajectories for basic P-box processes.

Table 2 Cases of $U^{\text{P.B.}}(t)$.

Case	$U^{\text{P.B.}}(t)$
1	$U^{\text{P.B.}}(t) = 4W_1^{\text{P.B.}}(t) - 2$
2	$U^{\text{P.B.}}(t) = 4W_2^{\text{P.B.}}(t) - 2$
3	$U^{\text{P.B.}}(t) = 1.5W_3^{\text{P.B.}}(t)$
4	$U^{\text{P.B.}}(t) = W_4^{\text{P.B.}}(t) - 5$

ear transformations of the basic P-box processes defined by Eq. (42) to assess the proposed method.

The problem is solved in the period of 0–5 s. The variable-step RK solver is applied with a relative error tolerance smaller than 1×10^{-6}. The error bars of $V^{\text{P.B.}}(t)$ and the approximated CDF bounds at 5 s of the four cases are shown in Figs. 11–14, and the reference solutions are also presented. To further examine the error of the proposed method, compared to the reference solutions, the relative errors of the calculated error bars and CDF bounds, denoted by $\varepsilon_{\text{e.b.}}$ and ε_F respectively, are evaluated as follows:

$$\begin{cases} \varepsilon_{\text{e.b.}} = \text{mean}_{10}\left[\frac{1}{N_1}\sum_{i=1}^{N_1}\sqrt{\left(\frac{e(t_i)-e_{\text{ref}}(t_i)}{e_{\text{ref}}(t_i)}\right)^2}\right] \\ \varepsilon_F = \text{mean}_{10}\left[\frac{1}{N_2}\sum_{i=1}^{N_2}\sqrt{\left(F(x_i)-F_{\text{ref}}(x_i)\right)^2}\right] \end{cases} \tag{45}$$

where N_1 denotes the number of discrete instants of the reference solution and is equal to 10, $e(t_i)$ and $e_{\text{ref}}(t_i)$ denote the lower and upper bounds of the error bars at t_i for the proposed method and MC-based method, respectively; and N_2 denotes the amount of discretization of the CDF, which is 10000, $F(x_i)$ and $F_{\text{ref}}(x_i)$ denote the value of CDF bounds at x_i for the proposed method and MC-based method. $\text{mean}_{10}[\cdot]$ indi-

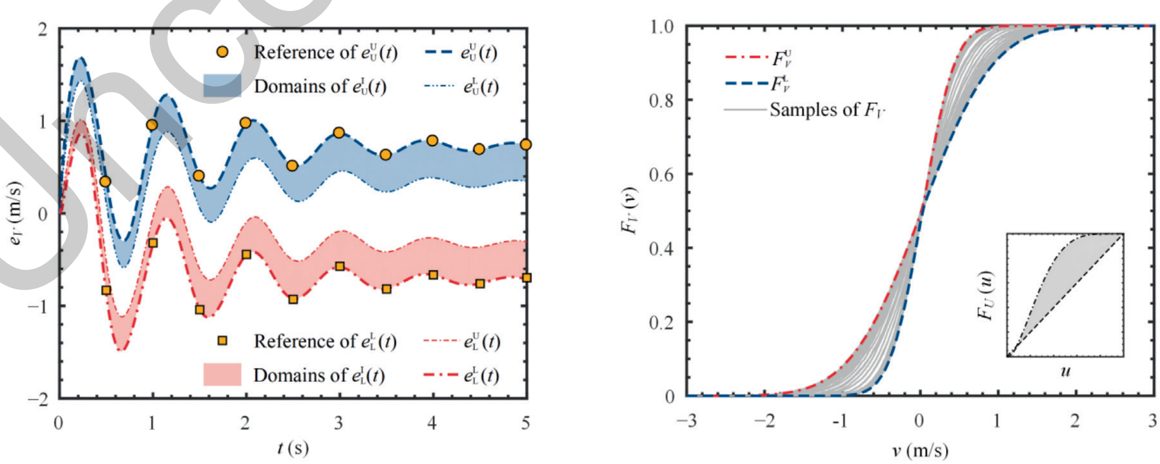

(a) Variation in error bar of $V^{\text{P.B.}}$ with time.

(b) Approximation of P-box of $V^{\text{P.B.}}$ at 5 s.

Fig. 11 Results of a duffing oscillator analysis for Case 1.

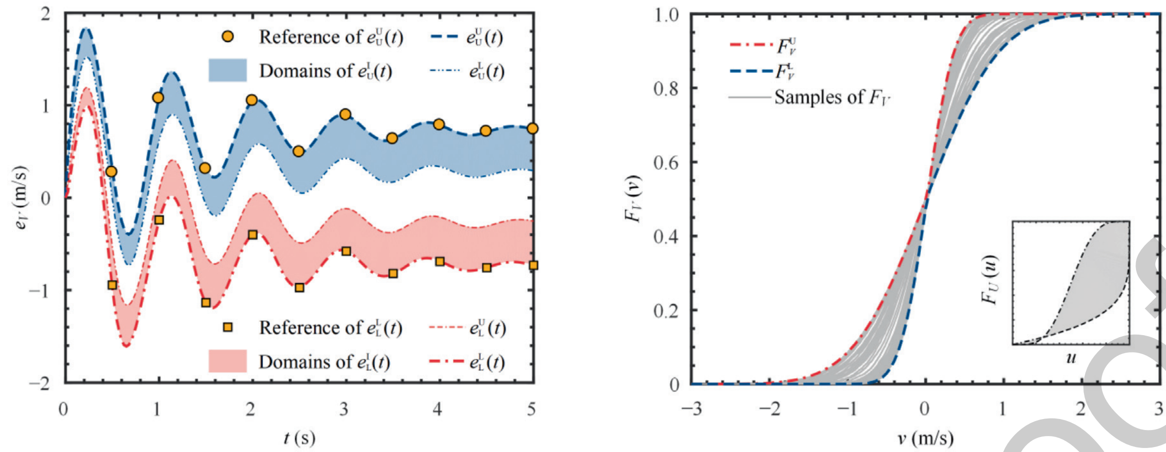

(a) Variation in error bar of $V^{\text{P.B.}}$ with time.   (b) Approximation of P-box of $V^{\text{P.B.}}$ at 5 s.

Fig. 12 Results of duffing oscillator analysis for Case 2.

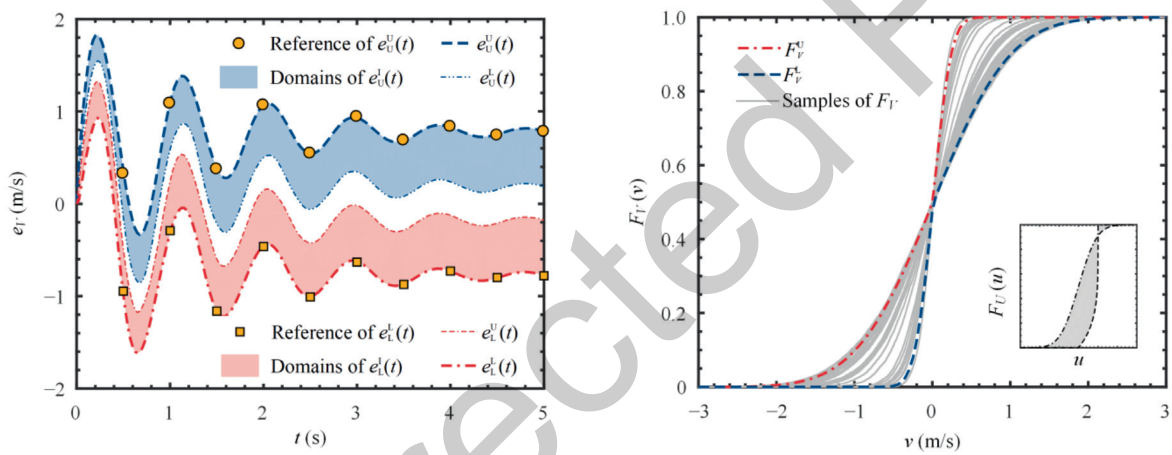

(a) Variation in error bar of $V^{\text{P.B.}}$ with time.   (b) Approximation of P-box of $V^{\text{P.B.}}$ at 5 s.

Fig. 13 Results of duffing oscillator analysis for Case 3.

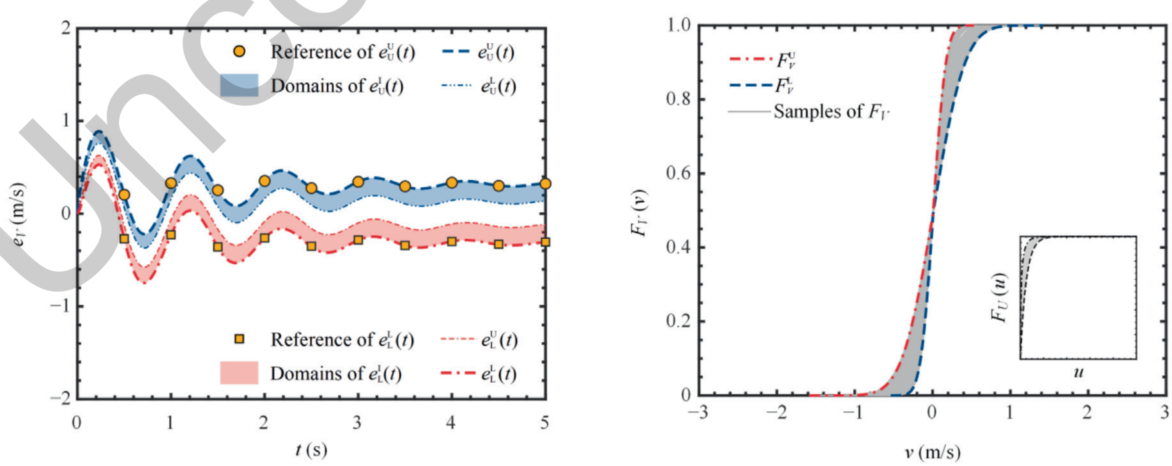

(a) Variation in error bar of $V^{\text{P.B.}}$ with time.   (b) Approximation of P-box of $V^{\text{P.B.}}$ at 5 s.

Fig. 14 Results of a duffing oscillator analysis for Case 4.

Table 3 Precision and efficiency of the proposed method in calculating $V^{\text{P.B.}}(t)$ of duffing oscillator analysis.

Characteristic		Value			
		Case 1	Case 2	Case 3	Case 4
Errors relative to the reference solutions (%)	$e_{\text{U}}^{\text{U}}(t)$ of $V^{\text{P.B.}}(t)$	1.32	1.20	1.34	0.91
	$e_{\text{L}}^{\text{L}}(t)$ of $V^{\text{P.B.}}(t)$	0.81	0.55	1.32	0.75
	$F_V^{\text{U}}(v, 5)$	0.25	0.26	1.48	0.56
	$F_V^{\text{L}}(v, 5)$	0.31	0.25	1.65	0.38
Computation time (s)	Reference solutions	$> 1.25 \times 10^5$			
	Proposed method	75.50	72.84	74.05	71.61

cates that the errors are evaluated by the mean of 10-time repetitions.

The relative errors of $e_{\text{U}}^{\text{U}}(t)$ and $e_{\text{L}}^{\text{L}}(t)$ of $V^{\text{P.B.}}(t)$, and the errors of the CDF bounds at 5 s, i.e., $F_V^{\text{U}}(v, 5)$ and $F_V^{\text{L}}(v, 5)$, are calculated, as shown in Table 3. Of note, all errors are less than 2%. Therefore, in terms of precision, the proposed method performs well in these cases. The proposed method only requires about 0.06% of the time to obtain the reference solutions. Finally, the CDF bounds of $V^{\text{P.B.}}(t)$ at 5 s, presented in Fig. 11(b), Fig. 12(b), Fig. 13(b), and Fig. 14(b), show that the responses are approximate parametric Gaussian P-box processes. This also holds for Case 4, with very skewed distributions.

The precision of the proposed method under different nonlinearities is also investigated in this example. The proposed method is tested in the duffing oscillator analysis based on the different values of the coefficient of the cubic term (ε = 1, 2, 5, 10, 20, and 50) for Case 1. The relative errors during the calculation of $V^{\text{P.B.}}(t)$ are presented in Table 4, and the results show that the error of the proposed method does not vary significantly when the nonlinearity of the problems changes.

4.1.2. Vehicle ride analysis

In the second example, a two-degree-of-freedom quarter-car model[30,32,33] presented in Eq. (46) is analyzed, and the corresponding schematic is shown in Fig. 15.

$$\begin{cases} \dot{x}_{\text{s}} = v_{\text{s}} \\ \dot{x}_{\text{u}} = v_{\text{u}} \\ \dot{v}_{\text{s}} = -\frac{1}{m_{\text{s}}}\left(c_{\text{s}}(v_{\text{s}} - v_{\text{u}}) + k_{\text{s}}(x_{\text{s}} - x_{\text{u}}) + K_{\text{s}}(x_{\text{s}} - x_{\text{u}})^3\right) \\ \dot{v}_{\text{u}} = \frac{1}{m_{\text{u}}}\left(c_{\text{s}}(v_{\text{s}} - v_{\text{u}}) + k_{\text{s}}(x_{\text{s}} - x_{\text{u}}) + K_{\text{s}}(x_{\text{s}} - x_{\text{u}})^3\right. \\ \qquad \left. + k_{\text{t}}(x_{\text{r}} - x_{\text{u}}) + K_{\text{t}}(x_{\text{r}} - x_{\text{u}})^3\right) \end{cases} \tag{46}$$

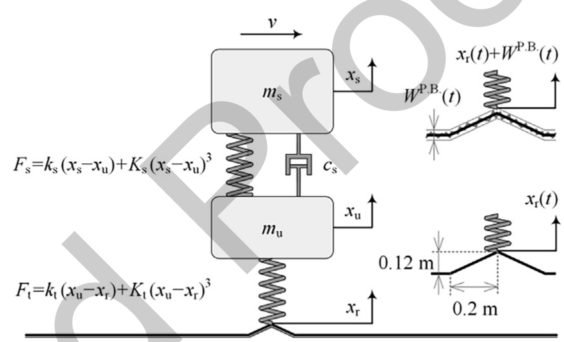

Fig. 15 Schematic of a quarter-car model with two degrees of freedom and roughness of road.

where x_{s} and v_{s} denote the sprung displacement and velocity, respectively; x_{u} and v_{u} denote the unsprung displacement and velocity, respectively, the initial condition is given as $[x_{\text{s}}(t_0), x_{\text{u}}(t_0), v_{\text{s}}(t_0), v_{\text{u}}(t_0)]^{\text{T}} = [0, 0, 0, 0]^{\text{T}}$, the sprung mass m_{s} and unsprung mass m_{u} are equal to 400 kg and 60 kg, respectively, the suspension damping rate c_{s} is equal to 1000, the linear stiffness characteristics of the suspension and tire, k_{s} and k_{t}, are equal to 1.5×10^4 and 2×10^5, respectively, and the cubic stiffness characteristics of the suspension and tire, K_{s} and K_{t}, are equal to 1.5×10^6 and 2×10^7, respectively.

It is supposed that the vehicle drives through a standard triangular roadblock at a speed v = 10 m/s. Then, x_{r} is computed as follows:

$$x_{\text{r}} = \begin{cases} 6t, & 0 \leqslant t < 0.02 \\ 0.24 - 6t, & 0.02 \leqslant t < 0.04 \\ 0, & t \geqslant 0.04 \end{cases} \tag{47}$$

Table 4 Relative errors in calculating $V^{\text{P.B.}}(t)$ for Case 1 with different values of ε.

Characteristics	Errors relative to the reference solutions (%)					
	ε = 1	ε = 2	ε = 5	ε = 10	ε = 20	ε = 50
$e_{\text{U}}^{\text{U}}(t)$ of $V^{\text{P.B.}}(t)$	1.32	1.39	1.88	1.09	1.77	1.43
$e_{\text{L}}^{\text{L}}(t)$ of $V^{\text{P.B.}}(t)$	0.81	1.13	0.76	1.07	1.39	2.44
$F_V^{\text{U}}(v, 5)$	0.25	0.27	0.36	0.21	0.25	0.29
$F_V^{\text{L}}(v, 5)$	0.31	0.26	0.17	0.27	0.29	0.37

Table 5 Cases of $W^{\text{P.B.}}(t)$.

Case	$W^{\text{P.B.}}$
1	$W^{\text{P.B.}}(t) = 6\times10^{-3}W_1^{\text{P.B.}}(t) - 3\times10^{-3}$
2	$W^{\text{P.B.}}(t) = 6\times10^{-3}W_2^{\text{P.B.}}(t) - 3\times10^{-3}$
3	$W^{\text{P.B.}}(t) = 2.25\times10^{-3}W_3^{\text{P.B.}}(t)$
3	$W^{\text{P.B.}}(t) = 2\times10^{-3}W_4^{\text{P.B.}}(t) - 1\times10^{-2}$

Afterward, the standard triangular roadblock is considered to be rough. Under the distribution-free P-box process model, due to additional roughness $W^{\text{P.B.}}(t)$, $x_{\text{r}}(t)$ is transformed into a P-box process $X_{\text{r}}^{\text{P.B.}}(t)$ as follows:

$$X_{\text{r}}^{\text{P.B.}}(t) = x_{\text{r}}(t) + W^{\text{P.B.}}(t) \tag{48}$$

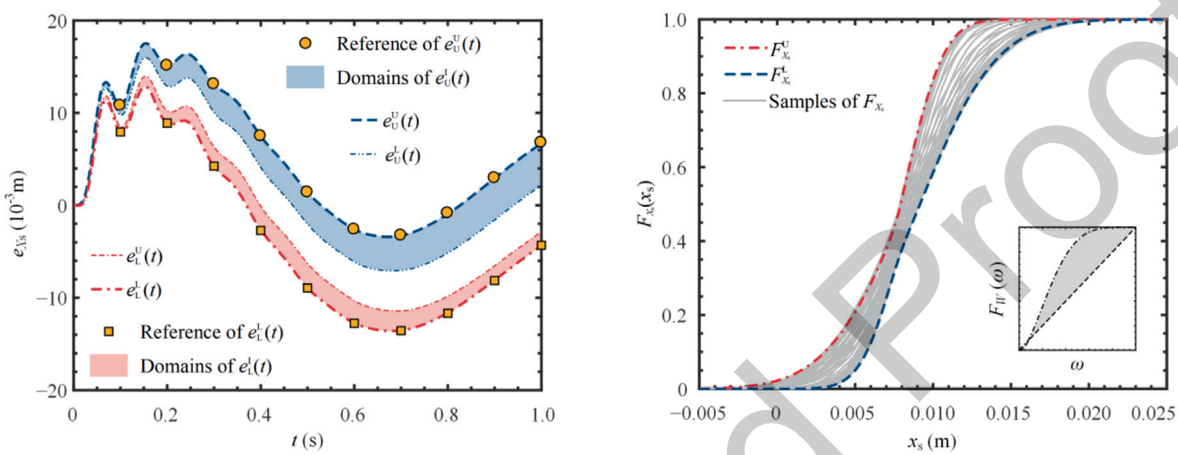

(a) Variation in error bar of XP.B. s with time.

(b) Approximation of P-box of XP.B. s at 0.3 s.

Fig. 16 Results of vehicle ride analysis for Case 1.

Table 6 Precision and efficiency of the proposed method in calculating $X_{\text{s}}^{\text{P.B.}}(t)$ for vehicle ride analysis.

Characteristic		Value			
		Case 1	Case 2	Case 3	Case 4
Errors relative to the reference solutions (%)	$e_{\text{U}}^{\text{U}}(t)$ of $X_{\text{s}}^{\text{P.B.}}(t)$	0.46	0.93	0.97	0.99
	$e_{\text{L}}^{\text{L}}(t)$ of $X_{\text{s}}^{\text{P.B.}}(t)$	0.60	0.24	0.58	0.57
	$F_{X_s}^{\text{U}}(x_s, 0.3)$	0.70	0.48	0.49	1.99
	$F_{X_s}^{\text{L}}(x_s, 0.3)$	0.28	0.75	1.14	0.75
Computation time (s)	Reference solutions	$> 1.45\times10^5$			
	Proposed method	87.47	89.13	90.63	87.94

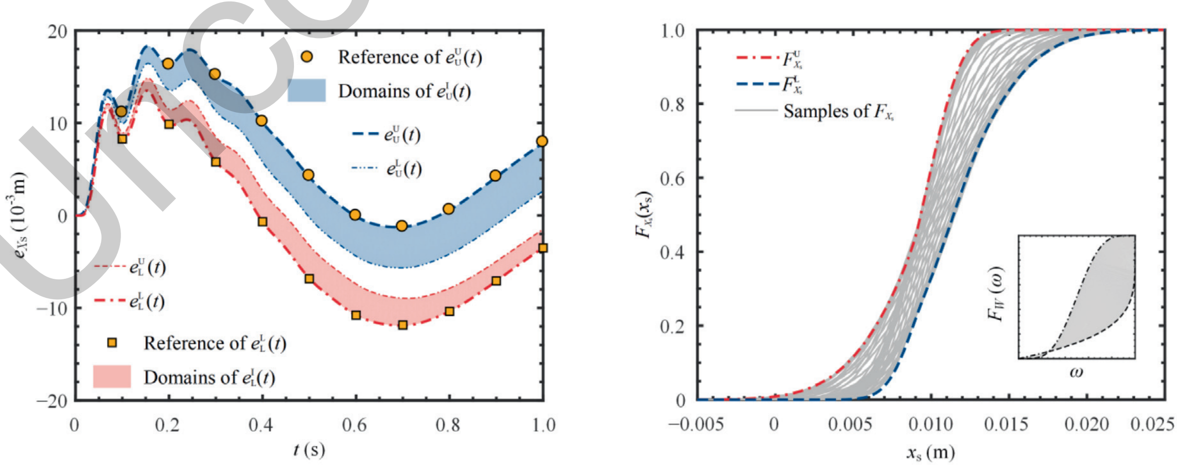

(a) Variation in error bar of XP.B. s with time.

(b) Approximation of P-box of XP.B. s at 0.3 s.

Fig. 17 Results of vehicle ride analysis for Case 2.

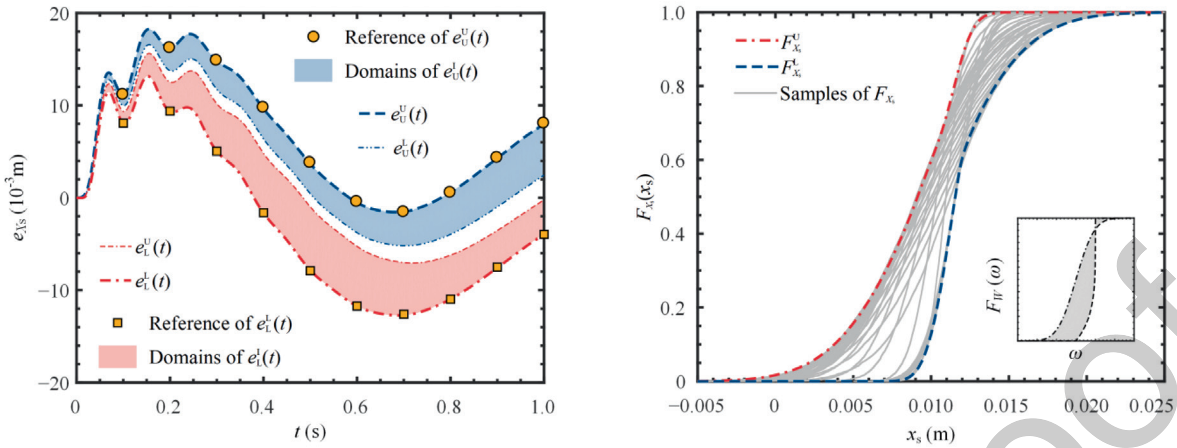

(a) Variation in error bar of XP.B. s with time. (b) Approximation of P-box of XP.B. s at 0.3 s.

Fig. 18 Results of vehicle ride analysis for Case 3.

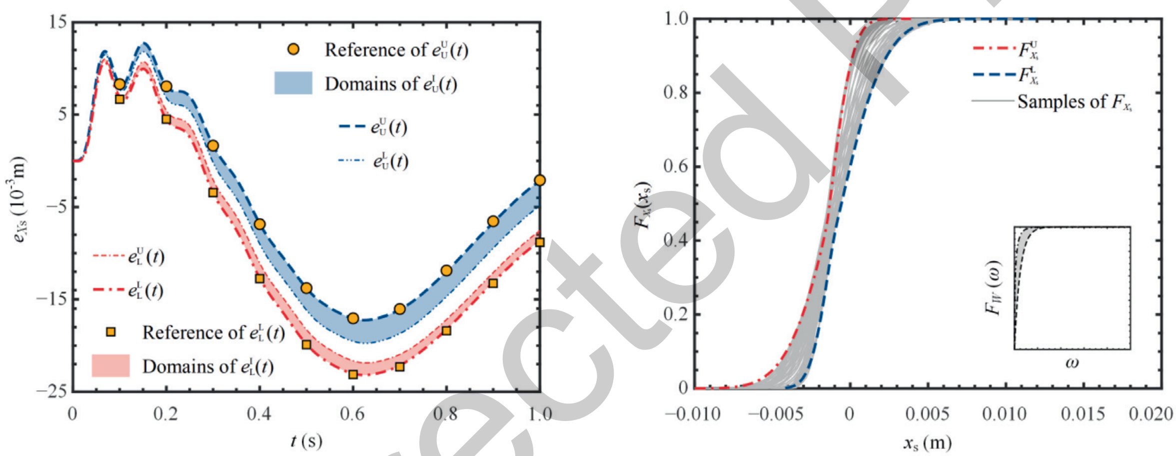

(a) Variation in error bar of XP.B. s with time. (b) Approximation of P-box of XP.B. s at 0.3 s.

Fig. 19 Results of vehicle ride analysis for Case 4.

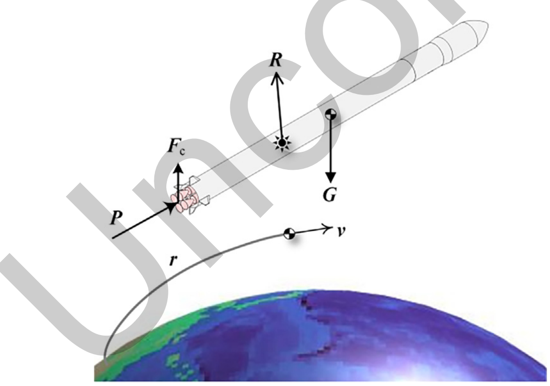

Fig. 20 Concept of the launch-vehicle-flight-dynamic model.

Four cases of $W^{\text{P.B.}}(t)$, as shown in Table 5, are obtained by using the linear transformations of the basic P-box processes defined by Eq. (42) to assess the proposed method.

Subsequently, after neglecting the effect of $W^{\text{P.B.}}(t)$ on the three-order term, the problem of nonlinear dynamics with the P-box process can be defined as follows:

$$\begin{cases} \dot{X}_s^{\text{P.B.}}(t) = V_s^{\text{P.B.}}(t) \\ \dot{X}_u^{\text{P.B.}}(t) = V_u^{\text{P.B.}}(t) \\ \dot{V}_s^{\text{P.B.}}(t) = f_s \\ \dot{V}_u^{\text{P.B.}}(t) = f_u + \frac{k_t}{m_u} W^{\text{P.B.}}(t) \end{cases} \tag{49}$$

where, f_s and f_u denote the nonlinear functions of v_s and v_u in Eq. (46), respectively.

The problem is solved in a period of 0–1 s, and a variable-step RK solver is applied with a relative error tolerance smaller than 1×10^{-4}. The error bars of $X_s^{\text{P.B.}}(t)$ and their approximated CDF bounds at 0.3 s for the four cases are shown in Fig. 16 to Fig. 19. The relative errors of $e_U^U(t)$ and $e_L^L(t)$ of $X_s^{\text{P.B.}}(t)$, as well as the errors of the CDF bounds at 0.3 s, i.e., $F_{X_s}^U(x_s, 0.3)$, and $F_{X_s}^L(x_s, 0.3)$, are calculated, as shown in Table 6. Of note, all error values are less than 1.2%. This indi-

Table 7 Basic parameters of launch vehicle.

Parameter		Symbol	Value
Total launch vehicle	Total mass (t)	m_{LV}	35.40
	Total length (m)	L	18.26
	Maximum diameter (m)	D	1.67
Substage 1	Substage mass (t)	m_1	22.68
	Propellent mass (t)	m_{p1}	20.80
	Propulsion (kN)	P_1	912
	Working time (s)	t_1	61.60
Substage 2	Substage mass (t)	m_2	7.05
	Propellent mass (t)	m_{p2}	6.25
	Propulsion (kN)	P_2	270
	Working time (s)	t_2	65.20
Substage 3	Substage mass (t)	m_3	3.65
	Propellent mass (t)	m_{p3}	3.32
	Propulsion (kN)	P_3	155
	Working time (s)	t_3	59.6

cates that the proposed method demonstrated good precision. Nevertheless, the proposed method requires less than 0.07% of the time required for obtaining the reference solutions. This shows that the proposed method is more efficient in terms of computational time. Finally, the responses are approximate parametric Gaussian P-box processes as shown in Fig. 16(b), Fig. 17(b), Fig. 18(b), and Fig. 19(b). Although, for Case 4, the relative error of $F^{\mathrm{U}}_{X_{\mathrm{s}}}(x_{\mathrm{s}}, 0.3)$ is close to 2%, the Gaussian assumption provides a satisfactory accuracy of the error bars in this case.

4.2. Application in uncertainty propagation of LV ascent trajectory

The concept of the LV-flight-dynamic model is illustrated in Fig. 20. The corresponding three-degree-of-freedom dynamic equations are expressed in a vector form presented in Eq. (50), which describes the motion of the center of mass of an LV.

$$\begin{cases} \dot{\boldsymbol{v}} = \frac{1}{m_{\mathrm{LV}}}(\mathrm{G} + \mathrm{R} + \mathrm{P} + \mathrm{F_c}) \\ \dot{\mathrm{r}} = \mathrm{v} \end{cases} \tag{50}$$

where $\mathrm{v} = [v_x,\ v_y,\ v_z]^{\mathrm{T}}$ denotes the velocity vector of the LV, $\mathrm{r} = [x,\ y,\ z]^{\mathrm{T}}$ denotes the position vector of the center of mass of the LV, m_{LV} denotes the mass of the LV, and $\boldsymbol{G}$, $\boldsymbol{R}$, $\boldsymbol{P}$, and $\mathrm{F_c}$ signify gravity, aerodynamic force, propulsion, and control

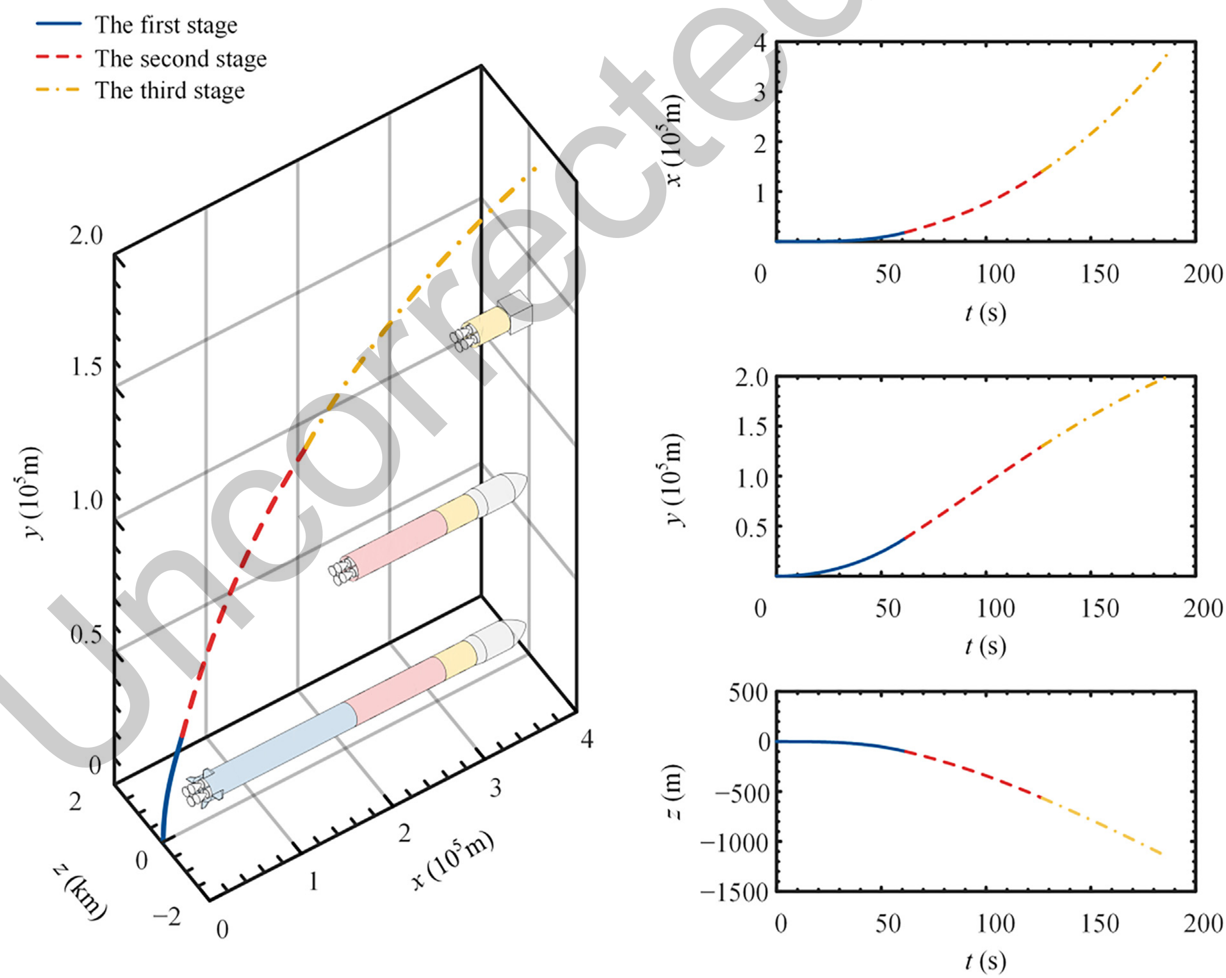

Fig. 21 Baseline trajectory of launch vehicle.

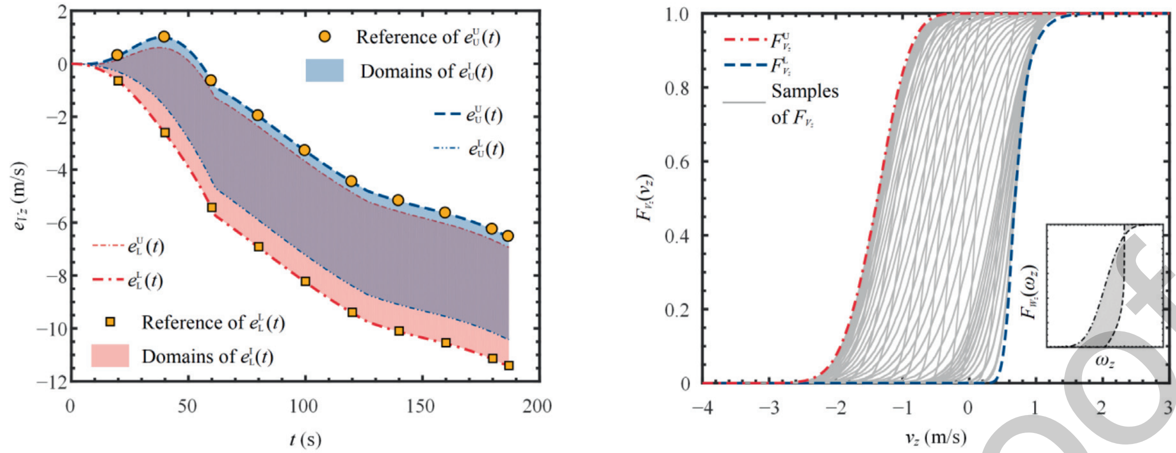

(a) Variation in the error bar of VP.B. z with time. (b) Approximation of the P-box of VP.B. z at 32.7 s.

Fig. 22 Results of launch-vehicle trajectory analysis of $V_z^{\text{P.B.}}(t)$.

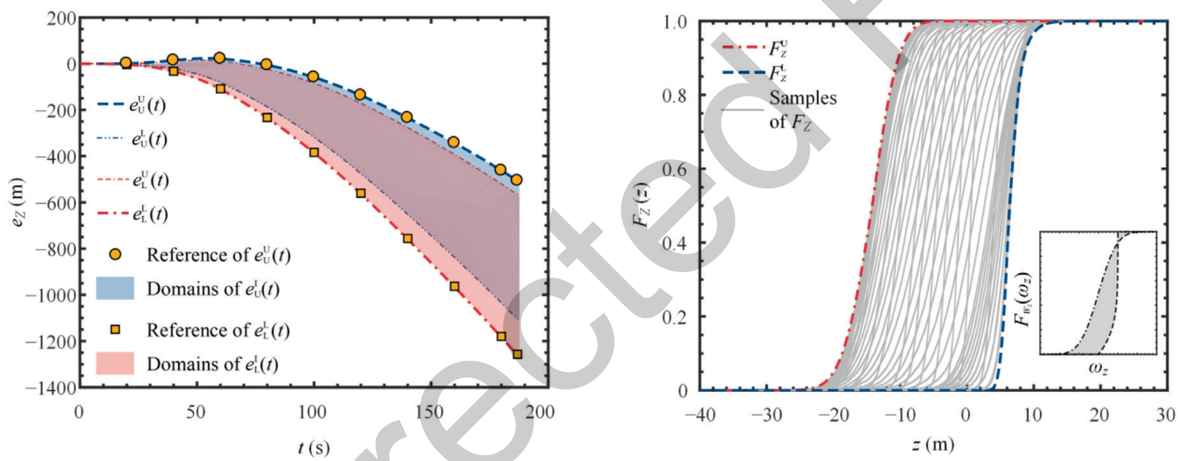

(a) Variation in error bar of $Z^{\text{P.B.}}$ with time. (b) Approximation of P-box of $Z^{\text{P.B.}}$ at 32.7 s.

Fig. 23 Results of launch-vehicle trajectory analysis of $Z^{\text{P.B.}}(t)$.

force on the LV, respectively. The detailed expansion of the model is presented in Appendix A.

In practical engineering, the values of the aforementioned forces cannot be obtained analytically and are always provided in the form of complex discrete tables. Therefore, the dynamic model is usually too complex to be modified arbitrarily and the calculation of LV trajectory is generally regarded as a black-box problem.

4.2.1. Uncertainty propagation problems

Consider a three-stage LV, with the basic parameters of this LV presented in Table 7 and other necessary parameters presented in Appendix B. The flight-program angle and control program formulated for flying the LV, according to a certain trajectory, are presented in Eq. (51). Based on these parameters, the baseline trajectory is simulated, as shown in Fig. 21.

$$\varphi_{\text{PR}}(t)=\begin{cases}\frac{\pi}{2}, & 0\,\text{s}\leqslant t<10\,\text{s}\\ \frac{\pi}{2}+\left(\frac{\pi}{2}-\frac{\pi}{60}\right)\left[\left(\frac{t-10}{150}\right)^2-2\left(\frac{t-10}{150}\right)\right], & 10\,\text{s}\leqslant t<160\,\text{s}\\ \frac{\pi}{60}, & t>160\,\text{s}\end{cases} \tag{51}$$

The actual flight of the LV will usually be affected by various uncertainties.[62,63] Among these uncertainties, the most common time-varying uncertainty is the atmospheric environment. At an earlier phase of design, because precise atmosphere information is usually unavailable, the P-box process model is chosen to describe the uncertainties.

Let $\mathrm{x}=[\mathrm{v}^{\mathrm{T}},\mathrm{r}^{\mathrm{T}}]^{\mathrm{T}}$, then, the dynamic model presented in Eq. (50) is expressed as follows:

$$\dot{\mathrm{x}}=\mathrm{f}(\mathrm{x},t) \tag{52}$$

Table 8 The precision and efficiency of the proposed method in calculating $V_z^{\mathrm{P.B.}}(t)$ and $Z^{\mathrm{P.B.}}(t)$ for launch-vehicle trajectory analysis.

Characteristic		Value
Errors relative to the reference solutions (%)	$e_{\mathrm{U}}^{\mathrm{U}}(t)$ of $V_z^{\mathrm{P.B.}}(t)$	0.89
	$e_{\mathrm{L}}^{\mathrm{L}}(t)$ of $V_z^{\mathrm{P.B.}}(t)$	0.53
	$F_{V_z}^{\mathrm{U}}(v_z, 32.7)$	0.77
	$F_{V_z}^{\mathrm{L}}(v_z, 32.7)$	2.95
	$e_{\mathrm{U}}^{\mathrm{U}}(t)$ of $Z^{\mathrm{P.B.}}(t)$	2.22
	$e_{\mathrm{L}}^{\mathrm{L}}(t)$ of $Z^{\mathrm{P.B.}}(t)$	0.65
	$F_Z^{\mathrm{U}}(z, 32.7)$	0.79
	$F_Z^{\mathrm{L}}(z, 32.7)$	2.99
Computation time (s)	Reference solutions	$> 4.12 \times 10^6$
	Proposed method	7812.59

where $\mathrm{f}(\cdot)$ denotes the nonlinear vector function presented in Eq. (50), and t denotes the flight time. The wind causes additional acceleration due to the variations in aerodynamic forces. Therefore, the problem is formulated as follows:

$$\begin{aligned}\dot{\boldsymbol{X}}^{\mathrm{P.B.}}(t) &= \boldsymbol{f}\left(\boldsymbol{X}^{\mathrm{P.B.}}(t), t\right) \\ &\quad + \boldsymbol{B}(t)\left[W_x^{\mathrm{P.B.}}(t), W_y^{\mathrm{P.B.}}(t), W_z^{\mathrm{P.B.}}(t), 0, 0, 0\right]^{\mathrm{T}}\end{aligned} \tag{53}$$

where $\mathrm{X}^{\mathrm{P.B.}} = \left(\left[V_x^{\mathrm{P.B.}}, V_y^{\mathrm{P.B.}}, V_z^{\mathrm{P.B.}}, X^{\mathrm{P.B.}}, Y^{\mathrm{P.B.}}, Z^{\mathrm{P.B.}}\right]^{\mathrm{T}}\right)$ denote the vector comprising the LV velocities and positions, which is described as P-box processes, $W_x^{\mathrm{P.B.}}(t)$, $W_y^{\mathrm{P.B.}}(t)$, and $W_z^{\mathrm{P.B.}}(t)$ denote the additional accelerations in the three degrees of freedom described by the distribution-free P-box processes. Based on the linear transformations of the basic P-box processes defined by Eq. (42), $W_x^{\mathrm{P.B.}}(t)$, $W_y^{\mathrm{P.B.}}(t)$, and $W_z^{\mathrm{P.B.}}(t)$ are defined as follows:

$$\begin{cases} W_x^{\mathrm{P.B.}}(t) = 2 \times 10^{-2} W_1^{\mathrm{P.B.}}(t) - 1 \times 10^{-2} \\ W_y^{\mathrm{P.B.}}(t) = 2 \times 10^{-2} W_2^{\mathrm{P.B.}}(t) - 1 \times 10^{-2} \\ W_z^{\mathrm{P.B.}}(t) = 7.5 \times 10^{-3} W_3^{\mathrm{P.B.}}(t) \end{cases} \tag{54}$$

$\mathrm{B}(t)$ as the input matrix is expressed as follows:

$$\boldsymbol{B}_{(6\times3)}(t) = \begin{bmatrix} \boldsymbol{Q}_{(3\times3)} \\ \boldsymbol{O}_{(3\times3)} \end{bmatrix} \quad \boldsymbol{Q}_{(3\times3)} = \mathrm{diag}\left(c\frac{q}{m_{\mathrm{LV}}}\right) \tag{55}$$

where q denotes the dynamic pressure, and c denotes a constant coefficient equal to 8.785 m^2.

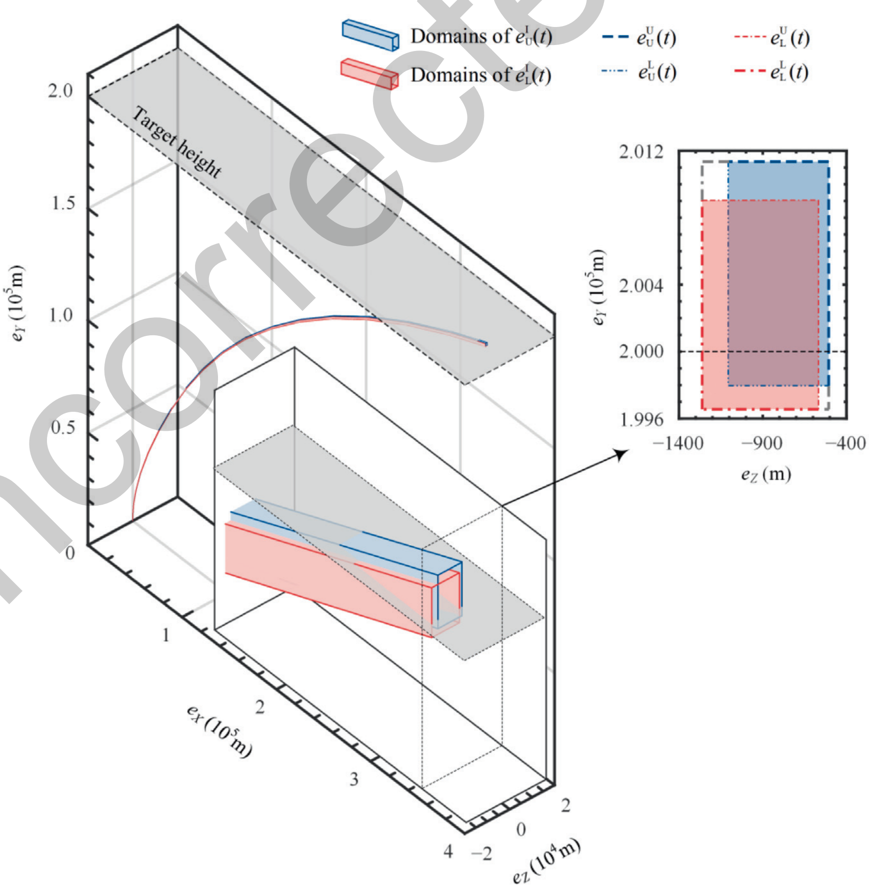

Fig. 24 Error bar of launch-vehicle ascent trajectory.

Please cite this article in press as: ZHANG L et al. An efficient uncertainty propagation method for nonlinear dynamics with distribution-free P-box processes, *Chin J Aeronaut* (2024), https://doi.org/10.1016/j.cja.2024.05.028

4.2.2. Results and discussion

The problem is solved in a period of 0–187 s. The variable-step RK solver is applied with a relative error tolerance smaller than 1×10^{-3}. The error bars of $V_z^{\text{P.B.}}(t)$ and $Z^{\text{P.B.}}(t)$, as well as their approximated CDF bounds at 32.7 s with maximum dynamic pressure, are shown in Fig. 22 and Fig. 23. The relative errors of $e_{\text{U}}^{\text{U}}(t)$ and $e_{\text{L}}^{\text{L}}(t)$ for $V_z^{\text{P.B.}}(t)$ and $Z^{\text{P.B.}}(t)$, as well as the CDF bounds at 32.7 s, i.e., $F_{V_z}^{\text{U}}(v_z,32.7)$, $F_{V_z}^{\text{L}}(v_z,32.7)$, $F_Z^{\text{U}}(z,32.7)$, and $F_Z^{\text{L}}(z,32.7)$, are calculated, as shown in Table 8. It can be observed that all errors are less than 3%, which satisfies the standards for the majority of practical engineering applications. The proposed method saves about 99.81% computational time compared to the MC-based approach. This shows that the proposed method is capable of handling the engineering black-box problem with satisfactory precision. Moreover, the response of this practical engineering system, i.e., the position and velocity of the LV, are still approximate parametric Gaussian P-box processes, as shown in Fig. 22(b) and Fig. 23(b).

Eventually, the entire LV trajectory under distribution-free P-box processes can be presented in the form of error bars, as shown in Fig. 24. The results efficiently obtained by the proposed method will provide valuable guidance for trajectory design under imprecision probabilistic information.

5. Conclusions

This work defines the Uncertainty Propagation (UP) problem of nonlinear dynamics with distribution-free P-box processes. This problem is meaningful for engineering applications, where only imprecise probabilistic information of dynamic excitations is available. Then, a novel method is presented to efficiently solve the UP problem.

(1) The proposed UP analysis method decouples the analyses of distribution-free P-box and stochastic analyses of nonlinear systems. As a result, a large portion of the computational cost is significantly reduced. Moreover, an extended Gaussian assumption in P-box form is considered, i.e., the system responses are approximately parametric Gaussian P-box processes. This assumption makes it possible to evaluate the CDF bounds of the response by only obtaining the interval bounds of means and variances.
(2) The tests performed in this work verify the accuracy of the proposed method. The calculation of error bars shows that compared to the reference solutions, the relative errors of the proposed method are typically less than 1%. The evaluation of CDF bounds shows that the proposed method reaches the relative errors of less than 3%. The Gaussian assumption is therefore effective in providing the error bars with satisfactory precision. In addition, the error of probability-bound evaluation based on the assumption is also acceptable.
(3) Based on the efficiency of the Chebyshev method for solving interval ODEs, the proposed method only required less than 0.2% calculation time of the reference solutions.
(4) The capacity of the method in solving complex black-box problems is demonstrated by the engineering application of the LV trajectory.

Declaration of competing interest

The authors declare that they have no known competing financial interests or personal relationships that could have appeared to influence the work reported in this paper.

Acknowledgements

The present work was supported by the major advanced research project of Civil Aerospace from State Administration of Science, Technology and Industry of China.

Appendix A. The detailed procedure of the MC-based method to calculate reference solutions is introduced as follows:

For simplicity, a one-dimension excitation, denoted by $W^{\text{P.B.}}(t)$, is considered as the example, where $W^{\text{P.B.}}(t)$ is defined based on a P-box $[F_W^{\text{L}}, F_W^{\text{U}}]$ using Eq. (3). As discussed in Section 3.2, the CDF realization set of $[F_W^{\text{L}}, F_W^{\text{U}}]$, denoted by S_F, can be obtained using Eq. (26), which is concisely expressed as follows:

$$\text{S}_F=\left\{F_W^{(k)}\middle|F_W^{(k)}\in\left[F_W^{\text{L}},F_W^{\text{U}}\right],k=1,2,\ldots,N_{\text{R}}\right\} \tag{A1}$$

where $F_W^{(k)}$ denotes the kth CDF realization of $[F_W^{\text{L}}, F_W^{\text{U}}]$ within S_F, and N_{R} is the total number of realizations within S_F.

Then, the problems presented in Eq. (8) and Eq. (12) can be formulated as finding the realizations that result in the bounds of the probabilistic characteristics of the system response, within S_F. For example, the calculation of CDF bounds can be formulated as follows:

$$\begin{cases}\text{F}_{\text{X}}^{\text{L}}(\text{x}|t)=\min\limits_{\substack{F_W^{(k)}\in\text{S}_F\\k=1,2,\ldots,N_R}}\text{F}_{\text{X}}\left(\text{x}\middle|F_W^{(k)},t\right)\\ \text{F}_{\text{X}}^{\text{U}}(\text{x}|t)=\max\limits_{\substack{F_W^{(k)}\in\text{S}_F\\k=1,2,\ldots,N_R}}\text{F}_{\text{X}}\left(\text{x}\middle|F_W^{(k)},t\right)\end{cases} \tag{A2}$$

For the kth CDF realization $F_W^{(k)}$, the calculation of the corresponding CDF of the system response can be achieved using $N_{\text{MC}}-$time MC simulations. Therefore, N_{MC} sample trajectories of $W^{\text{P.B.}}(t)$ corresponding to $F_W^{(k)}$, denoted by $\omega^{(k)}(t)$ ($\in\mathbb{R}^{N_{\text{MC}}}$, $\forall t$), are generated by using translation theory as follows:

$$\omega^{(k)}(t)=\left(F_W^{(k)}\right)^{-1}\circ\Phi(\eta(t)) \tag{A3}$$

where $\eta(t)$ ($\in\mathbb{R}^{N_{\text{MC}}}$, $\forall t$) denotes a vector function comprising N_{MC} sample trajectories of a standard white Gaussian noise process, which can be easily generated. Then, the MC simulations for obtaining CDF of the system response corresponding to $F_W^{(k)}$ can be achieved based on $\omega^{(k)}(t)$.

After performing the aforementioned calculation on $F_W^{(k)}$ from $k = 1$ to N_R, the set of CDF realizations for the system response is established. The solutions of Eq. (A2), termed reference solutions, can be found within the set. Finally, The flowchart illustrating the procedure to calculate reference solutions using MC simulations is presented in Fig. A1.

Fig. A1 Flowchart of the Monte-Carlo-based method.

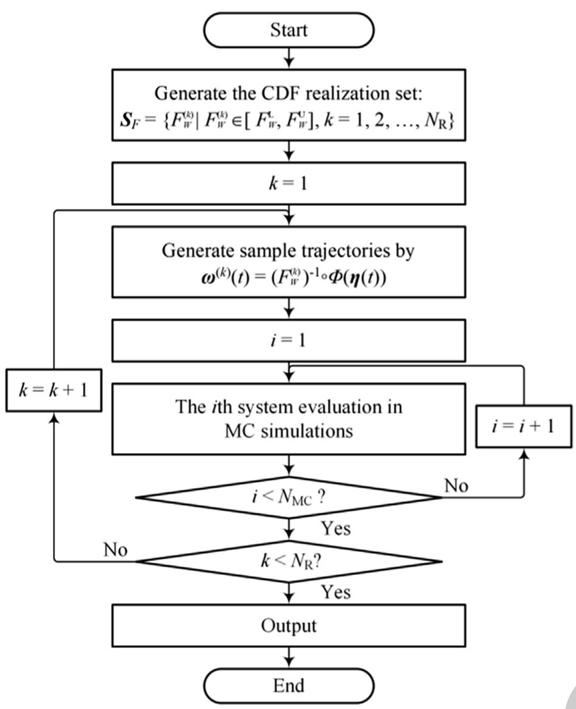

Appendix B. The detailed expansion of the LV-flight-dynamics model is expressed below:

$$\begin{cases} \begin{bmatrix} \dot{v}_x \\ \dot{v}_y \\ \dot{v}_z \end{bmatrix} = \frac{1}{m_{LV}} \boldsymbol{G}_B \begin{bmatrix} P - X_c \\ Y_c \\ Z_c \end{bmatrix} + \frac{1}{m_{LV}} \boldsymbol{G}_V \begin{bmatrix} -X \\ Y \\ Z \end{bmatrix} \\ + \frac{g_r}{r} \begin{bmatrix} x + R_{0x} \\ y + R_{0y} \\ z + R_{0z} \end{bmatrix} + \frac{g_{\omega e}}{\omega_e} \begin{bmatrix} \omega_{ex} \\ \omega_{ey} \\ \omega_{ez} \end{bmatrix} - \boldsymbol{A} \begin{bmatrix} x + R_{0x} \\ y + R_{0y} \\ z + R_{0z} \end{bmatrix} - \boldsymbol{B} \begin{bmatrix} v_x \\ v_y \\ v_z \end{bmatrix} \\ \begin{bmatrix} \dot{x} \\ \dot{y} \\ \dot{z} \end{bmatrix} = \begin{bmatrix} v_x \\ v_y \\ v_z \end{bmatrix} \end{cases} \tag{B1}$$

where m denotes the mass of LV, $[P,\ 0,\ 0]^T$ denotes the component of propulsion $\boldsymbol{P}$, $[X_c, Y_c, Z_c]^T$ denotes the components of control force $\boldsymbol{F}_c$, which is equal to $[0,\ 0,\ 0]^T$ in this work, and $[X, Y, Z]^T$ denotes the components of aerodynamic force $\boldsymbol{R}$, which are calculated as follows:

$$\begin{cases} X = C_x q S_R \\ Y = C_y^{\alpha} q S_R \alpha \\ Z = -C_y^{\alpha} q S_R \beta \end{cases} \tag{B2}$$

where α and β denote the angle of attack and sideslip angle, respectively. C_x denotes the drag coefficient, C_y^{α} represents the derivative of the lift coefficient with respect to α, S_R denotes the reference surface area, and q represents the dynamic pressure, which is computed as follows:

$$q = \frac{1}{2} \rho v^2 \tag{B3}$$

where ρ denotes the atmospheric density and v denotes the resultant velocity of the LV flight as:

$$v = \sqrt{v_x^2 + v_y^2 + v_z^2} \tag{B4}$$

G_B and G_V denote the coordinate-transform matrixes and are expressed as follows:

$$\begin{cases} \boldsymbol{G}_B = \begin{bmatrix} \cos\varphi cos\psi & -\sin\varphi & \cos\varphi\sin\psi \\ \sin\varphi\cos\psi & \cos\varphi & \sin\varphi\sin\psi \\ -\sin\psi & 0 & \cos\psi \end{bmatrix} \\ \boldsymbol{G}_V = \begin{bmatrix} \cos\theta cos\sigma & -\sin\theta & \cos\theta\sin\sigma \\ \sin\theta\cos\sigma & \cos\theta & \sin\theta\sin\sigma \\ -\sin\sigma & 0 & \cos\sigma \end{bmatrix} \end{cases} \tag{B5}$$

where, φ and ψ represent the pitch angle and yaw angle, respectively. These parameters describe the flight attitude of the LV. θ and σ denote the flight path angle and flight path azimuth angle, respectively. These parameters describe the flight direction of the LV. These angles are derived as follows:

$$\begin{cases} \theta = \arctan\frac{v_y}{v_x} \\ \sigma = -\arcsin\frac{v_z}{v} \\ \varphi = \theta + \alpha \\ \psi = \sigma + \beta \end{cases} \tag{B6}$$

Moreover, $\boldsymbol{A}$ and $\boldsymbol{B}$, in Eq. (B1) denote the matrixes to describe the inertial force caused by the rotation of the earth as follows:

$$\begin{cases} \boldsymbol{A} = \begin{bmatrix} \omega_{ex}^2 - \omega_e^2 & \omega_{ex}\omega_{ey} & \omega_{ex}\omega_{ez} \\ \omega_{ex}\omega_{ey} & \omega_{ey}^2 - \omega_e^2 & \omega_{ey}\omega_{ez} \\ \omega_{ex}\omega_{ez} & \omega_{ey}\omega_{ez} & \omega_{ez}^2 - \omega_e^2 \end{bmatrix} \\ \boldsymbol{B} = \begin{bmatrix} 0 & -2\omega_{ez} & 2\omega_{ey} \\ 2\omega_{ez} & 0 & -2\omega_{ex} \\ -2\omega_{ey} & 2\omega_{ex} & 0 \end{bmatrix} \end{cases} \tag{B7}$$

where ω_e denotes the earth-rotation rate and $[\omega_{ex},\ \omega_{ey},\ \omega_{ez}]^T$ denotes the components of the vector ω_e. $[R_{0x},\ R_{0y},\ R_{0z}]^T$ presented in Eq. (B1) represents the components of the vector R_0, which describes the position of the launch point. g_r and $g_{\omega e}$ represent the components of gravitational acceleration, and are calculated as follows:

$$\begin{cases} g_r = -\frac{\mu}{r^2}\left[1 + J\left(\frac{a_e}{r}\right)^2\left(1 - 5\sin^2\phi\right)\right] \\ g_{\omega e} = -2\frac{\mu}{r^2} J\left(\frac{a_e}{r}\right)^2 \sin\phi \end{cases} \tag{B8}$$

where μ and J denote the constant characteristics of gravity, a_e denotes the length of the semi-major axis of the earth under an ellipsoid model. The semi-minor axis is denoted as b_e. r denotes the geocentric distance of the LV and is calculated as follows:

$$r = \sqrt{(x + R_{0x})^2 + (y + R_{0y})^2 + (z + R_{0z})^2} \tag{B9}$$

ϕ denotes the geocentric latitudinal and is derived as follows:

$$\sin\phi = \frac{(x+R_{ox})\omega_{ex}+(y+R_{oy})\omega_{ey}+(z+R_{oz})\omega_{ez}}{r\omega_{e}} \tag{B10}$$

In addition, the flight height of the LV can also be obtained by using r and ϕ as follows:

$$h = r - \frac{a_e b_e}{\sqrt{a_e^2\sin^2\phi + b_e^2\cos^2\phi}} \tag{B11}$$

Finally, these equations are solved according to a given flight-program angle. Generally, they are provided in the following format:

$$\begin{cases} \varphi^* = \varphi_{PR}(t) \\ \psi^* = 0 \end{cases} \tag{B12}$$

To achieve the flight program, the corresponding α and β are expressed as follows:

$$\begin{cases} \alpha = A_\varphi[(\varphi_{PR} - \omega_{ez}t - \theta)] \\ \beta = A_\psi[(\varphi_{ex}\sin\varphi - \omega_{ey}\cos\varphi)t - \sigma] \end{cases} \tag{B13}$$

where A_φ and A_ψ represent constant coefficients. The values of the parameters involved in the dynamic model are presented in Table B1.

Table B1 Parameters of the dynamic model for launch-vehicle trajectory.

Parameter		Value
Launch point	R_{0x} (m)	0
	R_{0y} (m)	6,378,145
	R_{0z} (m)	0
Gravity	μ (m^3/s^2)	3.986×10^{14}
	J	1.624×10^{-3}
Aerodynamic coefficients	C_x	0.2
	C_y^α ($1/^\circ$)	0.07
	S_R (m^2)	2.19
Earth	a_e (m)	6,378,145
	b_e (m)	6,356,760
	ω_e (rad/s)	7.292×10^{-5}
	ω_{ex} (rad /s)	7.292×10^{-5}
	ω_{ey} (rad /s)	0
	ω_{ez} (rad /s)	0

References

1. Luo YZ, Yang Z. A review of uncertainty propagation in orbital mechanics. *Prog Aerosp Sci* 2017;**89**:23–39.
2. Fu C, Sinou JJ, Zhu WD, et al. A state-of-the-art review on uncertainty analysis of rotor systems. *Mech Syst Signal Process* 2023;**183**:109619.
3. Faes M, Moens D. Recent trends in the modeling and quantification of non-probabilistic uncertainty. *Arch Comput Meth Eng* 2020;**27**(3):633–71.
4. Beer M, Ferson S, Kreinovich V. Imprecise probabilities in engineering analyses. *Mech Syst Signal Process* 2013;**37**(1–2):4–29.
5. Shinozuka M. Monte Carlo solution of structural dynamics. *Comput Struct* 1972;**2**(5–6):855–74.
6. Geller DK. Linear covariance techniques for orbital rendezvous analysis and autonomous onboard mission planning. *J Guid Contr Dyn* 2006;**29**(6):1404–14.
7. Roberts J, Spanos P. *Random vibration and statistical linearization*. New York: Courier Corporation; 1990.
8. dos Santos KRM, Kougioumtzoglou IA, Spanos PD. Hilbert transform–based stochastic averaging technique for determining the survival probability of nonlinear oscillators. *J Eng Mech* 2019;**145**(10):4019079.
9. Kougioumtzoglou IA, Spanos PD. Response and first-passage statistics of nonlinear oscillators via a numerical path integral approach. *J Eng Mech* 2013;**139**(9):1207–17.
10. Zhu WQ. Nonlinear stochastic dynamics and control in Hamiltonian formulation. *Appl Mech Rev* 2006;**59**(4):230–48.
11. Li J. Probability density evolution method: background, significance and recent developments. *Probab Eng Mech* 2016;**44**:111–7.
12. Chen GH, Yang DX. A unified analysis framework of static and dynamic structural reliabilities based on direct probability integral method. *Mech Syst Signal Process* 2021;**158**:107783.
13. Chen HS, Chen GH, Meng Z, et al. Stochastic dynamic analysis of nonlinear MDOF systems under combined Gaussian and Poisson noise excitation based on DPIM. *Mech Syst Signal Process* 2022;**176**:109163.
14. Prabhakar A, Fisher J, Bhattacharya R. Polynomial chaos-based analysis of probabilistic uncertainty in hypersonic flight dynamics. *J Guid Contr Dyn* 2010;**33**(1):222–34.
15. Xiong FF, Chen SS, Xiong Y. Dynamic system uncertainty propagation using polynomial chaos. *Chin J Aeronaut* 2014;**27**(5):1156–70.
16. Jiang ZM, Li J. A new reliability method combining Kriging and probability density evolution method. *Int J Str Stab Dyn* 2017;**17**(10):1750113.
17. Bai ZW, Song SF. Physics-informed neural network for first-passage reliability assessment of structural dynamic systems. *Comput Struct* 2023;**289**:107189.
18. Das S, Tesfamariam S. Reliability assessment of stochastic dynamical systems using physics informed neural network based PDEM. *Reliab Eng Syst Saf* 2024;**243**:109849.
19. Wan ZQ, Chen JB, Tao WF, et al. A feature mapping strategy of metamodelling for nonlinear stochastic dynamical systems with low to high-dimensional input uncertainties. *Mech Syst Signal Process* 2023;**184**:109656.
20. Kong F, Spanos PD. Response spectral density determination for nonlinear systems endowed with fractional derivatives and subject to colored noise. *Probab Eng Mech* 2020;**59**:103023.
21. Lei SM, Ge YJ, Li Q, et al. Frequency-domain method for non-stationary stochastic vibrations of train-bridge coupled system with time-varying characteristics. *Mech Syst Signal Process* 2023;**183**:109637.
22. Julier S, Uhlmann J, Durrant-Whyte HF. A new method for the nonlinear transformation of means and covariances in filters and estimators. *IEEE Trans Autom Contr* 2000;**45**(3):477–82.
23. Park RS, Scheeres DJ. Nonlinear mapping of Gaussian statistics: theory and applications to spacecraft trajectory design. *J Guid Contr Dyn* 2006;**29**(6):1367–75.
24. Terejanu G, Singla P, Singh T, et al. Uncertainty propagation for nonlinear dynamic systems using Gaussian mixture models. *J Guid Contr Dyn* 2008;**31**(6):1623–33.
25. Ding C, Dang C, Valdebenito MA, et al. First-passage probability estimation of high-dimensional nonlinear stochastic dynamic systems by a fractional moments-based mixture distribution approach. *Mech Syst Signal Process* 2023;**185**:109775.
26. Huang DW, Wu F, Zhang S, et al. A high-performance calculation scheme for stochastic dynamic problems. *Mech Syst Signal Process* 2023;**189**:110073.
27. Weng YY, Lu ZH, Li PP, et al. Dynamic reliability analysis of structures under nonstationary stochastic excitations using tail-

modified extreme value distribution. *Mech Syst Signal Process* 2023;**198**:110424.

28. Elishakoff I, Elisseeff P, Glegg SAL. Nonprobabilistic, convex-theoretic modeling of scatter in material properties. *AIAA J* 1994;**32**(4):843–9.
29. Zadeh LA. Fuzzy sets as a basis for a theory of possibility. *Fuzzy Sets Syst* 1999;**100**:9–34.
30. Wu JL, Zhang YQ, Chen LP, et al. A Chebyshev interval method for nonlinear dynamic systems under uncertainty. *Appl Math Model* 2013;**37**(6):4578–91.
31. Wu JL, Luo Z, Zhang YQ, et al. Interval uncertain method for multibody mechanical systems using Chebyshev inclusion functions. *Int J Numer Meth Eng* 2013;**95**(7):608–30.
32. Li C, Chen BS, Peng HJ, et al. Sparse regression Chebyshev polynomial interval method for nonlinear dynamic systems under uncertainty. *Appl Math Model* 2017;**51**:505–25.
33. Wang LQ, Chen ZT, Yang GL. A polynomial chaos expansion approach for nonlinear dynamic systems with interval uncertainty. *Nonlinear Dyn* 2020;**101**(4):2489–508.
34. Wang LQ, Yang GL. An interval uncertainty propagation method using polynomial chaos expansion and its application in complicated multibody dynamic systems. *Nonlinear Dyn* 2021;**105**(1):837–58.
35. Wei S, Chu FL, Ding H, et al. Dynamic analysis of uncertain spur gear systems. *Mech Syst Signal Process* 2021;**150**:107280.
36. Fu C, Zheng ZL, Zhu WD, et al. Nonlinear vibrations of a rotor with support nonlinearities considering bounded uncertainties. *Nonlinear Dyn* 2022;**110**(3):2363–79.
37. Jiang C, Zhang QF, Han X, et al. Multidimensional parallelepiped model—a new type of non-probabilistic convex model for structural uncertainty analysis. *Num Meth Eng* 2015;**103**(1):31–59.
38. Ni BY, Jiang C, Han X. An improved multidimensional parallelepiped non-probabilistic model for structural uncertainty analysis. *Appl Math Model* 2016;**40**(7–8):4727–45.
39. Ni BY, Jiang C, Huang ZL. Discussions on non-probabilistic convex modelling for uncertain problems. *Appl Math Model* 2018;**59**:54–85.
40. Jiang C, Ni BY, Han X, et al. Non-probabilistic convex model process: a new method of time-variant uncertainty analysis and its application to structural dynamic reliability problems. *Comput Meth Appl Mech Eng* 2014;**268**:656–76.
41. Jiang C, Li JW, Ni BY, et al. Some significant improvements for interval process model and non-random vibration analysis method. *Comput Meth Appl Mech Eng* 2019;**357**:112565.
42. Jiang C, Liu NY, Ni BY. A Monte Carlo simulation method for non-random vibration analysis. *Acta Mechanica* 2017;**228**(7):2631–53.
43. Ni BY, Jiang C, Li JW, et al. Interval K-L expansion of interval process model for dynamic uncertainty analysis. *J Sound Vib* 2020;**474**:115254.
44. Zhang LC, Li CN, Su H, et al. A novel linear uncertainty propagation method for nonlinear dynamics with interval process. *Nonlinear Dyn* 2023;**111**(5):4425–50.
45. Faes MGR, Daub M, Marelli S, et al. Engineering analysis with probability boxes: a review on computational methods. *Struct Saf* 2021;**93**:102092.
46. Schöbi R, Sudret B. Global sensitivity analysis in the context of imprecise probabilities (p-boxes) using sparse polynomial chaos expansions. *Reliab Eng Syst Saf* 2019;**187**:129–41.
47. Liu HB, Jiang C, Xiao Z. Efficient uncertainty propagation for parameterized p-box using sparse-decomposition-based polynomial chaos expansion. *Mech Syst Signal Process* 2020;**138**:106589.
48. McKeand AM, Gorguluarslan RM, Choi SK. Stochastic analysis and validation under aleatory and epistemic uncertainties. *Reliab Eng Syst Saf* 2021;**205**:107258.
49. Li JW, Jiang C. A novel imprecise stochastic process model for time-variant or dynamic uncertainty quantification. *Chin J Aeronaut* 2022;**35**(9):255–67.
50. Faes MGR, Broggi M, Chen G, et al. Distribution-free P-box processes based on translation theory: definition and simulation. *Probab Eng Mech* 2022;**69**:103287.
51. Faes M, Moens D. Imprecise random field analysis with parametrized kernel functions. *Mech Syst Signal Process* 2019;**134**:106334.
52. Faes M, Valdebenito M, Moens D, et al. Bounding the first excursion probability of linear structures subjected to imprecise stochastic loading. *Comput Struct* 2020;**239**:106320.
53. Faes MGR, Valdebenito MA, Yuan XK, et al. Augmented reliability analysis for estimating imprecise first excursion probabilities in stochastic linear dynamics. *Adv Eng Softw* 2021;**155**:102993.
54. Faes MGR, Valdebenito MA, Moens D, et al. Operator norm theory as an efficient tool to propagate hybrid uncertainties and calculate imprecise probabilities. *Mech Syst Signal Process* 2021;**152**:107482.
55. Enszer JA, Lin YD, Ferson S, et al. Probability bounds analysis for nonlinear dynamic process models. *AlChE J* 2011;**57**(2):404–22.
56. Ni PH, Jerez DJ, Fragkoulis VC, et al. Operator norm-based statistical linearization to bound the first excursion probability of nonlinear structures subjected to imprecise stochastic loading. *ASCE-ASME J Risk Uncertainty Eng Syst, Part A: Civ Eng* 2022;**8**(1):4021086.
57. Wu JL, Luo Z, Zhang N, et al. A new uncertain analysis method and its application in vehicle dynamics. *Mech Syst Signal Process* 2015;**50–51**:659–75.
58. Wu JL, Luo L, Zhu B, et al. Dynamic computation for rigid–flexible multibody systems with hybrid uncertainty of randomness and interval. *Multibody Syst Dyn* 2019;**47**(1):43–64.
59. Taylor JH. *Handbook for the direct statistical analysis of missile guidance systems via CADET (Covariance analysis describing function technique)*. Massachusetts: Analytic Sciences Corporation; 1975.
60. Li QC, Fan YH, Xu HY, et al. A new approach for nonlinear transformation of means and covariances in direct statistical analysis of nonlinear systems. *IEEE Access* 2021;**9**:76738–49.
61. Wu JL, Luo Z, Zhang N, et al. A new sampling scheme for developing metamodels with the zeros of Chebyshev polynomials. *Eng Optim* 2015;**47**(9):1264–88.
62. Brevault L, Balesdent M. Uncertainty quantification for multidisciplinary launch vehicle design using model order reduction and spectral methods. *Acta Astronaut* 2021;**187**:295–314.
63. Zheng X, Ma N, Gao CS, et al. Propagation mechanism analysis of navigation errors caused by initial state errors for long-range vehicles. *Aerosp Sci Technol* 2017;**67**:378–86.

Please cite this article in press as: ZHANG L et al. An efficient uncertainty propagation method for nonlinear dynamics with distribution-free P-box processes, *Chin J Aeronaut* (2024), https://doi.org/10.1016/j.cja.2024.05.028